

GeCo: A Differentiable Geometric Consistency Metric for Video Generation

Leslie Gu¹ Junhwa Hur² Charles Herrmann² Fangneng Zhan³
 Todd Zickler¹ Deqing Sun² Hanspeter Pfister¹

¹Harvard University ²Google DeepMind ³Massachusetts Institute of Technology



Figure 1. **Geometric deformation detection on a generated video.** **Top:** Input frames; the white box marks the target frame for detection. **Middle:** Zoomed-in deformations. Red box: the front chess piece (indicated by the arrow) gradually moves toward the piece behind it until they merge into a single piece, with the merged region highlighted by a red dashed circle. Blue box: a bishop morphs into a queen. **Bottom:** Comparison of inconsistency maps. MEt3R [2] produces diffuse errors and fails to localize geometric shifts. WorldScore [10] captures inconsistencies but does not accurately localize surface deformations. Motion cue highlights non-rigid motion artifacts, but remains undefined in occlusion regions and thus misses occlusion inconsistency artifacts. GeCo fuses motion and depth cues, accurately pinpointing the artifacts while retaining coverage over visibility-inconsistent regions, yielding a sharp and interpretable inconsistency map.

Abstract

Generative video models can produce photorealistic outputs that violate basic 3D geometry, exhibiting non-rigid deformations and occlusion inconsistency (e.g., hallucinated content in disoccluded regions). These failures hinder downstream applications such as 3D asset creation and are poorly captured by existing metrics. We propose GeCo, a differentiable metric for static scenes that fuses motion and structure priors to produce interpretable, dense per-pixel maps of geometric consistency. We introduce WarpBench and OccluBench, two synthetic datasets that isolate deformation and occlusion-inconsistency effects, to validate

GeCo. Finally, we use GeCo to systematically benchmark recent video generation models and uncover common failure modes. Furthermore, we demonstrate its utility as a training-free guidance loss that significantly reduces geometric artifacts during generation. Project Page: <https://GeCo-GeoConsistency.github.io>.

1. Introduction

Recent generative video models have achieved remarkable photorealism but often violate basic 3D geometry. As the camera moves, nominally “rigid” objects can stretch, bend,

or melt. Models also exhibit occlusion inconsistency: after an object is occluded, it may reappear changed, and disoccluded regions may be hallucinated with new objects. These geometric inconsistency hinders downstream applications such as 3D asset creation and 3D world generation, motivating a metric that detects when and where inconsistency occurs—and ideally provides differentiable guidance to reduce it.

To this end, we propose investigating 3D consistency for static scenes captured by a moving camera, as a necessary step towards spatiotemporal (4D) consistency of general videos. If a model fails even in this controlled setting, it is unlikely to handle complex dynamics. Conversely, by addressing geometric consistency in static scenes, we establish the basis for consistent general video generation.

This restricted setup, however, remains challenging for existing metrics. Feature-based metrics prioritize semantic identity [2, 20, 21] and often overlook geometric deformations due to the inherent invariance of deep features. Sparse geometric metrics typically rely on keypoint matching and epipolar constraints [1, 46], but correspondences are unreliable or absent in occlusion regions—precisely where occlusion inconsistency occurs. Reprojection-error metrics depend on estimated camera poses and depths [10]; while effective at verifying coarse alignment, they are often too blunt to capture subtle, localized surface warping (Fig. 1).

In this paper, we propose GeCo, a dense, geometry-grounded diagnostic metric that jointly detects geometric deformation and occlusion-inconsistency artifacts. Rather than collapsing consistency into a single opaque scalar, GeCo produces interpretable, per-pixel error maps that localize geometric failures, from subtle surface distortions to major hallucinations. We leverage robust feed-forward models to extract optical flow, depth, and camera poses from generated videos, measure both motion and structure consistency, and fuse them into a unified scale-invariant map. With all components being differentiable, GeCo can be backpropagated through the generation pipeline to provide inference-time guidance.

To validate our design choices, we introduce two controlled benchmarks, WarpBench and OccluBench. WarpBench applies thin-plate-spline warps to real frames to mimic deformation, while OccluBench simulates occlusion-inconsistency artifacts. Experiments on these benchmarks show that motion cue and structure cue are complementary—motion is more sensitive to deformation, while structure better captures occlusion inconsistency artifacts—and that GeCo substantially outperforms the semantic baseline [2] in detecting geometric inconsistency.

We demonstrate the versatility of GeCo in two ways. First, as an evaluation metric, we benchmark state-of-the-art video models on a challenging suite of static scenes spanning object-centric, indoor, outdoor, and texturally com-

plex scenarios. Second, we leverage the differentiability of GeCo to derive an inference-time guidance scheme: optimizing GeCo during sampling significantly improves geometric consistency without model fine-tuning. Additionally, we show that this guidance suppresses spurious motion in common failure modes, mitigating erroneous dynamics in otherwise static regions.

To summarize, we make the following contributions:

- *GeCo*: A differentiable metric that jointly detects geometric deformation and occlusion-inconsistency artifacts in static scenes.
- *WarpBench & OccluBench*: Two controlled benchmarks that isolate deformation and occlusion-inconsistency artifacts to validate GeCo.
- *GeCo-Eval*: A static-scene evaluation suite for benchmarking video generation models with GeCo.
- *Inference-Time Guidance*: A training-free guidance framework that utilizes GeCo to reduce deformation artifacts and improve geometric consistency.
- *Failure-Mode Analysis*: An analysis of motion artifacts in recent t2v models, showing that GeCo guidance mitigates erroneous motion in representative failure modes.

2. Related Work

3D consistency metrics for visual generation. Most 3D-consistency metrics follow a two-stage pipeline: (i) establish inter-frame correspondences and (ii) compare cues on the matched content. Table 1 summarizes representative designs in terms of dense interpretability, deformation sensitivity, and occlusion-inconsistency awareness.

Correspondence matching. Correspondences are typically obtained via (a) sparse keypoints, (b) dense flow, or (c) 3D reconstruction-based warping (*i.e.*, reprojecting co-visible 3D points into the target view). Keypoint- and flow-based pipelines are inherently undefined in occlusion regions where no reliable matches exist; these regions are therefore commonly masked, directly ignoring occlusion inconsistency artifacts. Reconstruction-Warping is visibility-aware: co-visible points can be reprojected into both frames, exposing hallucinated content under inconsistent visibility.

Cue comparison. Given correspondences, methods compare either semantic features or geometric errors. Semantic features (*e.g.*, DINO [6], CLIP [30]) may under-penalize subtle geometric distortions when semantics are preserved. Epipolar-constraint cues (*e.g.*, symmetric epipolar distance [15], Sampson error [34]) are less sensitive when epipolar lines have similar orientations, as the epipolar error is insensitive to correspondence errors parallel to the epipolar line [46]. Depth cues depend on the accuracy of the underlying depth model and, when paired with 3D warping, may under-penalize deformations that remain close in

Table 1. **Comparison of GeCo and existing metrics.** We factor metrics into a two-stage pipeline: (i) correspondence matching and (ii) cue comparison. We report whether each method yields a dense, interpretable consistency map and whether it is diagnostic for subtle deformation and occlusion inconsistency artifacts.

Method	Correspondence	Cue	Dense	Deform.	Occlusion
TSED [46]	SIFT [27]	Symmetric epipolar distance [15]	✗	✓	✗
Nvidia Cosmos [1]	SuperPoint [9] & LightGlue [25]	Sampson error [34]	✗	✓	✗
VBench [20, 21]	None (frame-wise)	CLIP feature [30]	✗	✗	✗
MEt3R [2]	3D warping (DUST3R [38])	DINO feature [6]	✓	✗	✓
WorldScore [10]	Learnt flow (DROID-SLAM [35])	Reprojection error	✓	✓	✗
GeCo - Motion	Optical flow (UFM [50])	Residual motion	✓	✓	✗
GeCo - Structure	3D warping (VGST [37])	Reprojection error	✓	✗	✓
GeCo - Fused	Flow & 3D warping	Fused	✓	✓	✓

3D (*i.e.*, small depth residuals despite incorrect correspondences).

Representative methods. TSED [46] uses SIFT [27] with thresholded symmetric epipolar distance [15]; Nvidia Cosmos (Geometric Consistency) [1] uses SuperPoint [9] and LightGlue [25] with Sampson error [34]; and VBench (Background Consistency) [20, 21] compares global CLIP features [30] without explicit correspondence. MEt3R [2] uses DUST3R [38] warping with DINO features [6], while WorldScore (3D Consistency) [10] uses DROID-SLAM [35] to compute dense reprojection error from learned-flow correspondences. Our method fuses dense flow [50] and 3D warping [37] to produce dense, interpretable maps that capture both subtle deformation (residual motion) and occlusion inconsistency (reprojection error) within a unified metric.

Motion segmentation. Our pipeline share the similarity with the classical moving object or motion segmentation approaches [7, 19, 24, 40–42] when considering non-rigid local deformation as moving objects and disentangling it from static scenes. However, those methods are specifically trained for segmenting whole areas of moving objects instead of localizing only moving parts. On the other hands, our method can specifically pinpoints deformation parts.

3D consistent video generation. Toward 3D consistent video generation, recent approaches have explored multiple directions via joint video generation and geometry estimation [18, 48] or explicit spatio-temporal 3D cache [33]. While showing 3D consistent generation, the approaches typically require training datasets with 3D annotations (*e.g.* depth, pointmaps, camera pose) that are obtained by off-the-shelf methods [4, 35, 38, 43]. The annotations are often inaccurate, and it requires tremendous efforts on pre-processing. In contrast, we introduce a simple, training-free approach that improves 3D consistency of pretrained video model by using our metric as a guidance term.

Training-free guidance for diffusion models. A rich line of research explores training-free guidance for diffu-

sion models, where controllability is achieved at inference time without updating model parameters. Specifically, ControlVideo [49] adapts ControlNet [47] to the video counterpart in a training-free manner, enabling controllable text-to-video generation with structural consistency. Several works investigate guided sampling and inference-time optimization to steer diffusion trajectories toward desired semantics or constraints [3, 14]. A key observation across these methods is that diffusion models determine the global structure in the early denoising steps, with later steps refining details [22]. More recent efforts incorporate additional structural constraints through inference-time optimization. MotionPrompt [29] introduces optical-flow-guided prompt optimization to achieve flow-based motion consistency objectives. Motion Guidance [11] similarly achieves motion controllability by imposing flow-derived guidance directly on the denoising process.

3. GeCo: A Differentiable Geometric Consistency Metric for Video Generation

We introduce GeCo, a differentiable metric that measures geometric consistency in generated videos and apply it as a guidance signal to improve 3D consistency for video generation.

3.1. Metric for Geometric Consistency

To quantify geometric consistency in static scenes observed by a moving camera, GeCo employs a bottom-up design based on dense per-pixel correspondence. Motion consistency verifies if every pixel’s motion strictly satisfies the rigid motion induced by the camera, measured as the residual between observed optical flow and the expected rigid motion induced by camera. However, since visible geometry should remain invariant without objects suddenly appearing or disappearing, we also account for regions where flow correspondence naturally breaks down. To quantify it, we introduce a structure consistency metric as a complementary signal, which evaluates depth reprojection error to

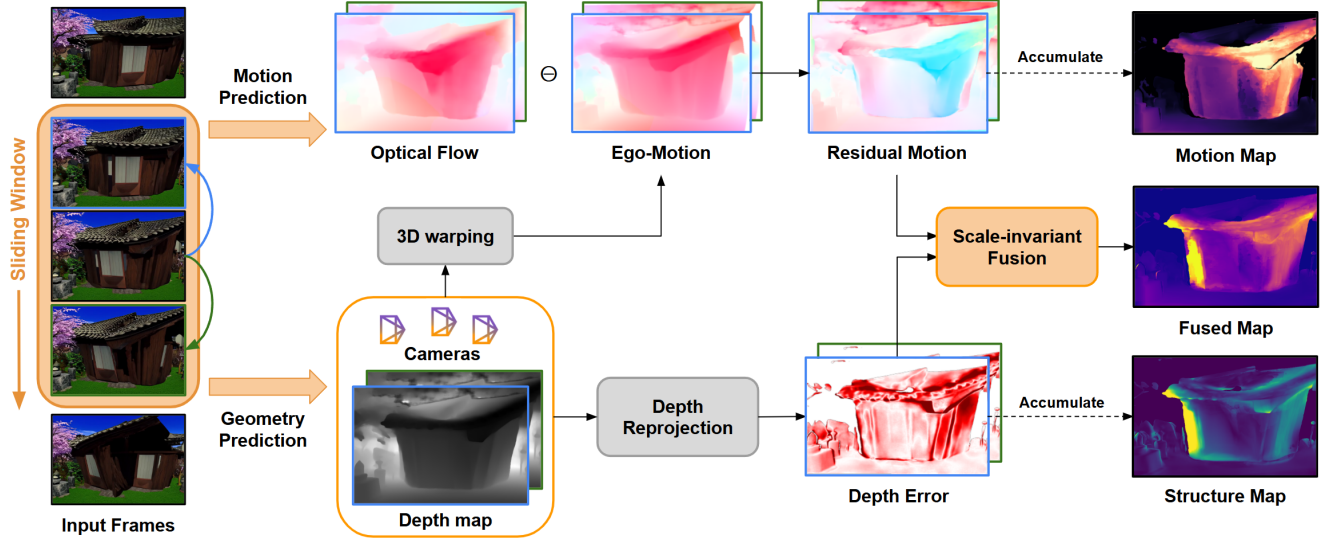


Figure 2. **GeCo pipeline.** Within a sliding window, we jointly estimate dense optical flow and 3D geometry (depth and camera pose) for frame pairs. We compute residual motion and depth errors and fuse them into scale-invariant inconsistency maps. Aggregation over the window localizes artifacts in the target frame, while motion and structure maps provide complementary diagnostics.

penalize artifacts such as sudden appearance or disappearance that optical flow cues cannot track.

Fig. 2 shows the pipeline for metric computation. GeCo processes an input video in a sliding window fashion. Given N frames in a window, we compute the metric for the center frame \mathbf{I}_c . For each pair $(\mathbf{I}_c, \mathbf{I}_i)$ with $i \in \{1, \dots, N\} \setminus \{c\}$, it computes two consistency metrics, motion consistency and structure consistency, and fuses them into a per-pixel error map for the center frame. This per-pixel map can localize where the deformation occurs in each image.

Motion consistency. Motion consistency measures the residual between optical flow and rigid motion induced by camera in the pixel space. Given two frames $(\mathbf{I}_c$ and \mathbf{I}_i), dense optical flow $\mathbf{F}_{\text{flow}}^{c \rightarrow i}$ is obtained by an off-the-shelf model [50]. For camera-induced motion, we use a geometry foundation model [37] to predict depth map \mathbf{D}_c , camera intrinsics \mathbf{K}_c (with focal lengths f_x, f_y), and relative pose $\mathbf{P}_{c \rightarrow i} = (\mathbf{R}, \mathbf{T})$. Then we get residual motion by subtracting optical flow by and rigid motion:

$$\mathbf{F}_{\text{residual}}(\mathbf{p}) = \mathbf{F}_{\text{flow}}^{c \rightarrow i}(\mathbf{p}) - \mathbf{F}_{\text{rigid}}(\mathbf{p}) \quad (1)$$

$$\mathbf{F}_{\text{rigid}}(\mathbf{p}) = \pi_{\mathbf{K}_i}(\mathbf{R}[\mathbf{D}_c(\mathbf{p}) \mathbf{K}_c^{-1} \tilde{\mathbf{p}}] + \mathbf{T}) - \mathbf{p}, \quad (2)$$

with $\tilde{\mathbf{p}}$ being the homogeneous coordinate of pixel \mathbf{p} and perspective projection $\pi_{\mathbf{K}}(\cdot)$ with intrinsics \mathbf{K} . The residual motion is computed only for co-visible pixels between the center frame and the rest frames, discarding occluded regions where optical flow is not reliable.

Structure consistency. Structure consistency evaluates geometric coherence to handle regions where optical flow is unreliable (e.g. occlusions). Given two frames \mathbf{I}_c and \mathbf{I}_i ,

we reproject the depth map \mathbf{D}_i into the viewpoint of \mathbf{I}_c using the estimated relative pose $\mathbf{P}_{i \rightarrow c}$ and intrinsics \mathbf{K}_i . This process yields a warped depth map $\mathbf{D}_{i \rightarrow c}$, utilizing z-buffering to resolve self-occlusions. The structure consistency at pixel \mathbf{p} is then defined as the residual between the predicted and reprojected depth:

$$\Delta z(\mathbf{p}) = \mathbf{D}_c(\mathbf{p}) - \mathbf{D}_{i \rightarrow c}(\mathbf{p}). \quad (3)$$

Scale-invariant fusion. Direct fusion of the two signals is non-trivial due to unit mismatch: motion consistency is in pixels, while structure consistency is in depth unit up to scale. To combine them, we normalize both signals into a dimensionless, scale-invariant space via the pinhole camera model. Let $(\Delta u, \Delta v) = \mathbf{F}_{\text{residual}}(\mathbf{p})$ be the flow residual and $\Delta z(\mathbf{p})$ be the depth residual. We define the normalized motion consistency $\mathbf{m}(\mathbf{p})$ and structure consistency $\mathbf{s}(\mathbf{p})$ as:

$$\mathbf{m}(\mathbf{p}) = \sqrt{\left(\frac{\Delta u}{f_x}\right)^2 + \left(\frac{\Delta v}{f_y}\right)^2}, \quad \mathbf{s}(\mathbf{p}) = \left| \frac{\Delta z(\mathbf{p})}{\mathbf{D}_c(\mathbf{p})} \right|. \quad (4)$$

We fuse these cues into a unified error map \mathbf{M}_{geo} for the center frame \mathbf{I}_c :

$$\mathbf{M}_{\text{geo}}(\mathbf{p}) = \sqrt{(\mathbb{1}_{\text{cov}}(\mathbf{p}) \cdot \mathbf{m}(\mathbf{p}))^2 + \mathbf{s}(\mathbf{p})^2}, \quad (5)$$

where $\mathbb{1}_{\text{cov}}$ is the co-visibility mask. This allows structure consistency to dominate in occluded regions (where $\mathbb{1}_{\text{cov}}=0$), while utilizing both metrics in co-visible areas to robustly localize deformation.

Temporal aggregation. For each center frame \mathbf{I}_c in a video, we average the pairwise error maps within its sliding window to obtain aggregated frame-level error maps

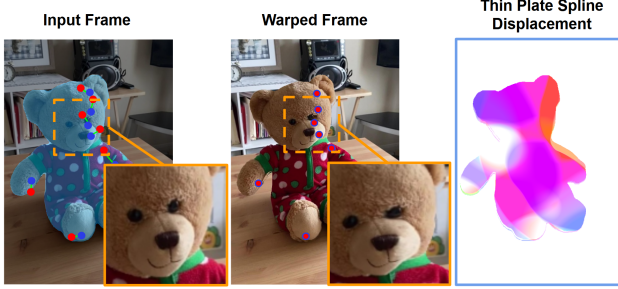


Figure 3. **WarpBench deformation process.** (Left) Input frame with foreground segmentation mask (cyan), sampled thin-plate spline (TPS) control points (red), and their destination points (blue). (Middle) Warped frame after the TPS deformation. (Right) Ground-truth dense displacement field from the deformation.

$\{\mathbf{m}_c, \mathbf{s}_c, \mathbf{M}_{\text{geo},c}\}$. We then compute the spatial mean of each map to define scalar frame-level scores. Finally, video-level metrics are obtained by averaging these frame-level scores over all frames in the sequence, yielding three per-video scalars, which we denote by $\mathcal{M}_{\text{motion}}$, $\mathcal{M}_{\text{struct}}$, and \mathcal{M}_{geo} for motion, structure, and fused geometric consistency, respectively.

3.2. Training-free Guidance with GeCo

Not only as an evaluation metric, GeCo serves as a differentiable guidance term to improve geometric consistency during video generation, without requiring model fine-tuning.

Building on CogVideoX-5B [44] and Frame Guidance [22], we update the latent \mathbf{z}_t at timestep t by minimizing our GeCo metric during sampling time:

$$\mathbf{z}_t \leftarrow \mathbf{z}_t - \eta_t \nabla_{\mathbf{z}_t} \mathcal{L}_{\text{geo}}(\hat{\mathbf{x}}_{0|t}^{\mathcal{I}}), \quad (6)$$

where η_t is the guidance scale and $\hat{\mathbf{x}}_{0|t}^{\mathcal{I}}$ represents the approximated clean frames. The loss \mathcal{L}_{geo} aggregates the error map \mathbf{M}_{geo} over a subset of frames \mathcal{I} and temporal offsets \mathcal{K} :

$$\mathcal{L}_{\text{geo}}(\hat{\mathbf{x}}^{\mathcal{I}}) = \frac{1}{|\mathcal{I}||\mathcal{K}|} \sum_{c \in \mathcal{I}} \sum_{k \in \mathcal{K}} \sum_{\mathbf{p} \in \Omega} \mathbf{M}_{\text{geo}}^{(c,k)}(\mathbf{p}), \quad (7)$$

where \mathcal{I} denotes the subset of guidance frames, \mathcal{K} defines the temporal offsets relative to each center frame $c \in \mathcal{I}$, and Ω represents the pixel domain.

As our metric requires clean input images, we estimate the clean latent $\hat{\mathbf{z}}_{0|t}$ from the current noisy state \mathbf{z}_t and predicted velocity \mathbf{v}_{θ} , then decode it via the decoder $D(\cdot)$:

$$\hat{\mathbf{z}}_{0|t} = \sqrt{\bar{\alpha}_t} \mathbf{z}_t - \sqrt{1 - \bar{\alpha}_t} \mathbf{v}_{\theta}(\mathbf{z}_t, t) \quad (8)$$

$$\hat{\mathbf{x}}_{0|t}^{\mathcal{I}} = D(\hat{\mathbf{z}}_{0|t})^{\mathcal{I}}, \quad (9)$$

Gradients are backpropagated through the frozen decoder and the GeCo pipeline to update \mathbf{z}_t , improving the geometric consistency (*i.e.*, lowering \mathcal{L}_{geo}) throughout the sampling process. All pretrained backbones used to compute depth [37] and flow [50] are frozen.



Figure 4. **OccluBench.** An example sequence where a region in the image center is (i) visible and empty, (ii) occluded, and (iii) re-revealed with a new object, forming a controlled sudden-appearance artifact.

To ensure efficiency and stability during sampling, we employ three strategies:

- Latent slicing [22] to decode only a small temporal window \mathcal{I} for guidance \mathcal{L}_{geo} computation, instead of using the full sequence.
- Recursive denoising [3, 28, 39] to repeat updates R times per step to improve convergence
- Time-travel [16] to re-noise the latent after updates, to mitigate accumulated sampling error.

4. Benchmark Datasets for GeCo Validation

While we have defined our metric, it is equally important to validate our design choices. To this end, we introduce two synthetic benchmark datasets, WarpBench and OccluBench, designed to simulate typical 3D inconsistency artifacts observed in generated videos.

4.1. WarpBench: Synthetic Deformation Dataset

Data generation. We construct WarpBench using clips from CO3D [32] (*CO3D-Warp*, object-centric) and ScanNet++ [8, 45] (*ScanNet-Warp*, indoor scenes). To simulate non-rigid deformation artifacts, we inject temporally smooth warps parameterized by thin-plate splines (TPS) into the foreground (Fig. 3). For each clip, we sample control points on the foreground and evolve their displacements temporally. We generate the warped frame via differentiable sampling and compute the ground-truth dense displacement field analytically. In total, WarpBench contains 200 clips (4,000 frames). We describe a detailed dataset generation process in the supplementary material.

Metric validation on WarpBench. We validate GeCo on WarpBench (comprising object-centric CO3D and indoor ScanNet) via two tasks: (*i*) frame-level anomaly detection, identifying a single warped frame within a clip, and

Table 2. **WarpBench: frame-level anomaly detection accuracy in %.** Higher is better. Both of our motion and fused metric shows their competitiveness on both benchmark datasets while MEt3R performs poorly.

Method	CO3D-Warp	ScanNet-Warp
MEt3R [2] (baseline)	6.82	15.38
Structure metric $\mathcal{M}_{\text{struct}}$	42.05	84.62
Motion metric $\mathcal{M}_{\text{motion}}$	71.59	89.23
Fused metric \mathcal{M}_{geo}	55.68	92.31

(ii) deformation localization, segmenting the precise region of deformation. We compare our three proposing metrics ($\mathcal{M}_{\text{motion}}$, $\mathcal{M}_{\text{struct}}$, and \mathcal{M}_{geo}) with the MEt3R [2] as well.

Frame-level anomaly detection. We randomly replace a single frame in a clip with its warped version, and the goal is to identify the anomalous frame. For each clip, we treat each metric as a frame-wise anomaly score and predict the anomalous frame as the one with the largest score in the clip (i.e., $\hat{t} = \arg \max_t \mathcal{M}(t)$). Tab. 2 shows that the Motion metric $\mathcal{M}_{\text{motion}}$ is the most reliable on CO3D-Warp and Fused metric \mathcal{M}_{geo} on ScanNet-Warp, by complementarily using both metrics. The Structure (depth) cue is informative for scenes but noisier for object-centric data. MEt3R performs very poorly, underscoring the difficulty of detecting subtle deformations with semantic features.

Deformation localization. This task evaluates the accuracy of localizing the deformed region. Given a pair of real and warped frame, each metric outputs a inconsistency map, and we compare against the ground-truth deformation mask. We report AP (%), IoU (%), and Spearman’s rank correlation coefficient (SRCC) (See supplementary for details) to measure detection quality, mask overlap, and rank correlation with the true deformation magnitude.

As shown in Tab. 3 (WarpBench columns), Motion is the strongest cue, consistently achieving the highest AP and IoU, which is designed to detect such deformation. MEt3R yields negative SRCC, indicating anti-correlation with deformation magnitude and highlighting the limitations of semantic feature-based metrics. While fusing depth does not surpass motion alone for pure deformations, it remains competitive.

4.2. OccluBench: Occlusion Inconsistency Dataset

Sudden appearance under occlusion. Generative models often struggle with object permanency during disocclusions (e.g. an object changes its appearance after being occluded). While optical flow inherently misses these errors due to a lack of correspondence, depth reprojection can detect the underlying 3D inconsistency. To validate the necessity of this depth cue, we introduce OccluBench: 30 clips (5,165 frames) featuring controlled sudden-appearance ar-

tifacts, where a region is occluded and then re-revealed containing a new, inconsistent object (Fig. 4). We provide ground-truth masks for these artifacts across 1,654 frames, annotated with SAM 2 [31].

We evaluate the artifact localization in the re-reveal frame for each metric. We report AP (%), IoU (%), and F1 (%). AP is threshold-free and implemented as ranking average precision. IoU and F1 are computed at the per-image best threshold, then macro-averaged across $N=60$ anchors. Results in Tab. 3 (OccluBench columns) validate our design choice: the Motion cue fails almost completely as it ignores the occlusion. The Structure cue effectively localizes the artifact. The Fused metric achieves the best overall performance, validating the necessity of combining depth with motion to handle complex occlusion scenarios.

5. Experiments

5.1. GeCo-Eval: Benchmark Suite for T2V Models

Benchmark design. We benchmark text-to-video models on geometric consistency using GeCo-Eval. To mirror downstream 3D applications, we design four scenarios: (i) object-centric scenes, (ii) indoor scenes, (iii) outdoor scenes, and (iv) appearance-complex scenes (e.g., characterized by high-frequency patterns, reflections, and thin structures). The suite consists of total 80 prompts describing static scenes, split into slow and fast camera trajectories to stress-test both subtle breathing artifacts and multi-view coherence under large viewpoint changes.

Models. We evaluate recent, state-of-the-art models: 2 commercial ones (Sora 2 [5], Veo 3.1 [12]) and 4 open-source ones (WAN 2.2 [36], HunyuanVideo [23], LTX-Video [13], and CogVideoX variants [17, 44]). We generate 4 videos per each prompt across 8 models, yielding 2,560 videos total.

Evaluation protocol. To ensure fair comparison across different models with their own native generation settings, we evaluate GeCo on overlapping ≈ 3 -second windows resampled to a maximum of $f_{\text{eval}}=8$ FPS. Within each window, we compute motion, structure, and fused scores averaged over pixels with valid depth and covisibility. Final clip-level scores are derived from the frame-weighted average of these windows, and we report the mean across all 320 clips (80 prompts \times 4 seeds) per model.

Motion magnitude. High consistency scores can stem from valid geometry or simply a lack of motion in generated videos. To disambiguate these, we also include a normalized motion statistic per each model. We quantify motion using the per-frame optical flow magnitude normalized by the image diagonal (m_t). We define Total Motion as the cumulative normalized optical flow ($\sum m_t$) over the clip, representing the total amount of visual change inde-

Table 3. **Combined Results on WarpBench and OccluBench.** We validate our metrics on both benchmarks, WarpBench for deformation and OccluBench for sudden appearance. Higher is better for all metrics. Our fused metric \mathcal{M}_{geo} shows its effectiveness on both benchmarks.

Method	WarpBench						OccluBench		
	CO3D-Warp			ScanNet-Warp			Sudden Appearance		
	AP (%) \uparrow	IoU (%) \uparrow	SRCC \uparrow	AP (%) \uparrow	IoU (%) \uparrow	SRCC \uparrow	AP (%) \uparrow	IoU (%) \uparrow	F1 (%) \uparrow
MEt3R [2] (baseline)	16.26	15.95	-0.176	30.34	33.13	-0.351	46.51	33.97	48.57
Structure metric $\mathcal{M}_{\text{struct}}$	25.64	3.20	0.079	51.71	14.11	0.183	62.36	51.46	66.96
Motion metric $\mathcal{M}_{\text{motion}}$	64.90	44.48	0.581	87.12	52.36	0.706	4.43	5.85	8.62
Fused metric \mathcal{M}_{geo}	60.63	41.69	0.554	82.70	48.87	0.547	83.48	69.83	81.74

Table 4. **GeCo-Eval across scenarios.** Per-model mean motion inconsistency, structure inconsistency, and Fused GeCo scores (lower is better) together with Total Motion (%) and Mean Motion (%/s; mean \pm std over clips). Commercial models (top block) and open-source models (bottom block) are compared across four scenarios: (a) object-centric, (b) indoor navigation, (c) outdoor reconstruction, and (d) challenging appearance-complex scenes. Darker green cells indicate the best Motion/Structure/Fused scores among commercial models, lighter green cells indicate the best scores among open-source models, and red cells highlight models with very low Total Motion and Mean Motion, where a high consistency score may be partially achieved by under-shooting motion (near-static generations).

(a) Object-centric						(b) Indoor					
Model	Motion \downarrow	Structure \downarrow	Fused \downarrow	Total Motion (%)	Mean Motion (%/s)	Model	Motion \downarrow	Structure \downarrow	Fused \downarrow	Total Motion (%)	Mean Motion (%/s)
Sora 2	0.019	0.103	0.110	24.97 \pm 42.68	6.29 \pm 10.76	Sora 2	0.027	0.218	0.226	71.12 \pm 123.63	17.93 \pm 31.17
Veo 3.1	0.010	0.075	0.077	52.48 \pm 34.84	6.59 \pm 4.38	Veo 3.1	0.032	0.185	0.196	136.06 \pm 113.56	17.10 \pm 14.27
WAN 2.2	0.028	0.101	0.109	87.11 \pm 91.10	17.42 \pm 18.22	WAN 2.2	0.036	0.235	0.244	106.79 \pm 111.28	21.36 \pm 22.26
JunyuanVideo	0.012	0.070	0.073	34.29 \pm 35.06	6.43 \pm 6.57	JunyuanVideo	0.017	0.139	0.143	122.06 \pm 139.96	22.89 \pm 26.24
CogVideoX1.5	0.010	0.080	0.082	9.16 \pm 11.55	1.83 \pm 2.31	CogVideoX1.5	0.010	0.113	0.116	14.22 \pm 14.12	2.84 \pm 2.82
CogVideoX-5B	0.023	0.065	0.073	59.81 \pm 77.73	19.94 \pm 25.91	CogVideoX-5B	0.024	0.147	0.153	57.14 \pm 68.53	19.05 \pm 22.84
CogVideoX-2B	0.017	0.056	0.062	30.57 \pm 34.77	10.19 \pm 11.59	CogVideoX-2B	0.025	0.107	0.115	47.14 \pm 43.65	15.71 \pm 14.55
LTX-Video	0.006	0.028	0.030	13.01 \pm 20.07	3.25 \pm 5.02	LTX-Video	0.014	0.031	0.038	21.27 \pm 33.21	5.32 \pm 8.30
(c) Outdoor						(d) Appearance-complex					
Model	Motion \downarrow	Structure \downarrow	Fused \downarrow	Total Motion (%)	Mean Motion (%/s)	Model	Motion \downarrow	Structure \downarrow	Fused \downarrow	Total Motion (%)	Mean Motion (%/s)
Sora 2	0.031	0.290	0.297	63.62 \pm 97.34	16.04 \pm 24.54	Sora 2	0.042	0.168	0.181	56.58 \pm 90.84	14.26 \pm 22.90
Veo 3.1	0.021	0.208	0.214	161.61 \pm 137.62	20.31 \pm 17.29	Veo 3.1	0.023	0.165	0.172	90.61 \pm 80.47	11.39 \pm 10.11
WAN 2.2	0.046	0.299	0.312	159.98 \pm 179.82	32.00 \pm 35.96	WAN 2.2	0.043	0.168	0.187	104.36 \pm 123.70	20.87 \pm 24.74
JunyuanVideo	0.025	0.293	0.300	118.64 \pm 150.64	22.25 \pm 28.24	JunyuanVideo	0.022	0.101	0.110	53.65 \pm 58.44	10.06 \pm 10.96
CogVideoX1.5	0.012	0.057	0.061	24.44 \pm 35.76	4.89 \pm 7.15	CogVideoX1.5	0.016	0.523	0.528	11.28 \pm 10.04	2.26 \pm 2.01
CogVideoX-5B	0.026	0.120	0.128	81.52 \pm 86.97	27.17 \pm 28.99	CogVideoX-5B	0.045	0.161	0.177	53.35 \pm 54.24	17.78 \pm 18.08
CogVideoX-2B	0.015	0.072	0.077	44.15 \pm 39.60	14.72 \pm 13.20	CogVideoX-2B	0.023	0.072	0.083	39.47 \pm 38.52	13.16 \pm 12.84
LTX-Video	0.018	0.084	0.090	27.32 \pm 37.89	6.83 \pm 9.47	LTX-Video	0.010	0.046	0.050	13.51 \pm 29.38	3.38 \pm 7.34

pendent of FPS. We also define Mean Motion as the total motion divided by duration (Total Motion/ S), with clip length S , representing the average speed of the camera. These statistics allow us to assess geometric scores relative to the video’s dynamic intensity.

Analysis. Tab. 4 benchmarks all models on our metrics, in the context of motion magnitude. Commercial models demonstrate superior robustness: Veo 3.1 consistently outperforms Sora 2, yielding lower inconsistency scores across all scenarios while sustaining comparable or significantly higher Total Motion. This indicates that Veo 3.1 preserves 3D fidelity without compromising temporal dynamism. In contrast, open-source models exhibit a pronounced trade-off between dynamism and consistency. LTX-Video and CogVideoX1.5-5B achieve high consistency scores but operate in a constrained low-motion regime (3–6 \times lower Total Motion), often generating conservative trajectories to

minimize deformation. Conversely, WAN 2.2 and JunyuanVideo produce highly dynamic content but suffer from significant geometric degradation, particularly in complex scenes. CogVideoX-2B/5B occupy an intermediate position, suggesting that maintaining structural integrity under substantial camera motion remains a critical challenge for current open-weight architectures.

5.2. GeCo-Guided Inference

We apply GeCo as a training-free guidance to CogVideoX-5B, as in Sec. 3.2. We evaluate this on a subset of 45 prompts sampled from our benchmark scenarios. For each prompt, we generate paired videos (with and without guidance) using identical random seeds and sampling hyperparameters (details are in supplementary). We evaluate the generated videos on our metrics as well as MEt3R [2] to quantify the change in multiple metrics.

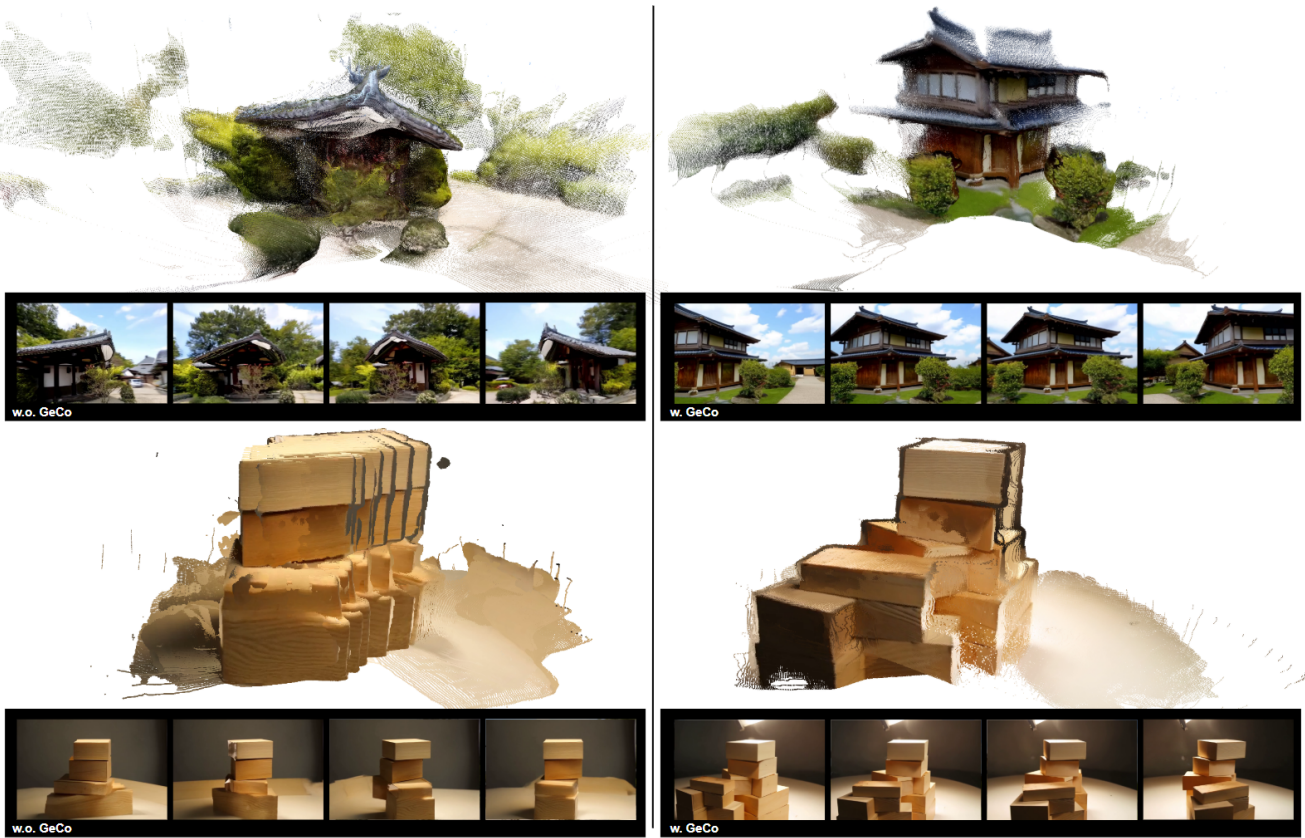


Figure 5. **GeCo guidance improves geometric consistency for 3D reconstruction.** Top: 3D reconstructions from videos generated by CogVideoX-5B without (left) and with GeCo guidance (right). Bottom: corresponding video frames. Both guided videos yield cleaner geometry with fewer deformation and drifting artifacts across views, which enables higher reconstruction quality.

Table 5. **GeCo-guided sampling improves geometric consistency.** We compare CogVideoX-5B with and without GeCo guidance on a set of 45 prompts. Lower is better for all metrics.

Method	MEt3R [2] \downarrow	Structure \downarrow	Motion \downarrow	Fused \downarrow
Without guidance	0.100	0.136	0.032	0.147
With guidance	0.098	0.126	0.029	0.135

As in Tab. 5, GeCo guidance consistently reduces geometric deformation. All scores improve, by reductions in both structure and motion errors and improvement on 3D consistency. Importantly, MEt3R is marginally lowered, confirming that MEt3R does not effectively capture the improvement. Qualitative results in Fig. 5 demonstrate that guided videos yield cleaner 3D reconstructions with reduced drifting and fewer artifacts around thin structures.

5.3. Findings on Video Generation Models

The Globe That Can't Be Stopped. We identify a persistent failure mode where video models struggle to generate static objects under camera motion, likely due to training

data bias (*e.g.*, spinning globes). As shown in Fig. 6, models consistently animate the globe despite static prompts, while GeCo correctly identifies this spurious object motion as a geometric inconsistency. We believe a possible reason for the failure mode is the bias in training data, where most examples of globes appear in motion, leading models to conflate object persistence with deformation or drift.

Freezing the Spurious Motion. To empirically evaluate our assumption, we test prompts which should be sparse in video training data such as "a camera orbiting a dog that has no motion." Models typically fail to keep the subject rigid. However, by using GeCo as a guidance term, we can strongly suppress this non-ego motion. As illustrated in Fig. 7, our guidance effectively freezes the subject, creating a bullet-time effect where the camera orbits while the object remains rigid.

6. Conclusion

In this work, we introduce GeCo, an interpretable consistency metric that fuses differentiable optical flow and depth priors to localize geometric artifacts in



Figure 6. **“The Globe That Can’t Be Stopped.”** A common failure mode that models consistently make the globe rotate despite static prompts. GeCo localizes this spurious object motion on the globe surface, clearly separating it from the intended egocentric camera motion.

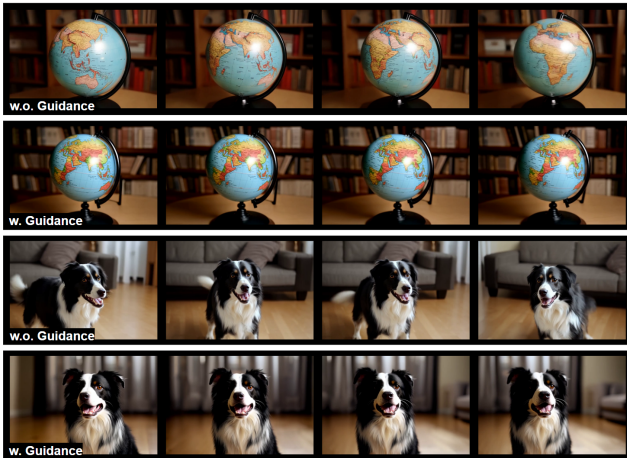


Figure 7. **Stopping the globe and freezing the dog with GeCo-guidance.** We compare video generations for prompts specifying a camera orbiting a nominally static globe (top rows) and a static dog (bottom rows). Without guidance, the model introduces spurious object motion, causing the globe to spin and the dog to move. Applying GeCo guidance effectively suppresses this non-ego motion, enforcing geometric consistency where the subject remains rigid while the camera orbits, producing a “bullet-time” effect.

generated videos. We develop WarpBench and OccluBench—synthetic benchmarks for non-rigid deformation and occlusion inconsistency artifacts—to validate the metric, and build GeCo-Eval, a large-scale benchmark evaluating geometric consistency across six state-of-the-art text-to-video models (commercial and open-source) over four scenarios and 2,560 clips.

We also use GeCo as a differentiable loss for training-free guidance, producing cleaner geometry with fewer deformations and drifting artifacts and improving 3D reconstruction quality. Finally, we analyze recurring failure modes triggered by simple prompts (e.g., a rigid globe under camera motion or orbiting around a stationary dog), observe them across most models, and show that GeCo-based guidance suppresses spurious motion that violates the prompt. Overall, our results position GeCo as both a diagnostic and control tool, and underscore geometric consistency as a persistent challenge—motivating geometry-

aware evaluation and guidance for future video generation systems.

Acknowledgement. This project is supported in part by NSF grant CRCNS-2309041. The views and conclusions contained herein are those of the authors and do not represent the official policies or endorsements of these institutions.

References

- [1] Niket Agarwal, Arslan Ali, Maciej Bala, Yogesh Balaji, Erik Barker, Tiffany Cai, Prithvijit Chattopadhyay, Yongxin Chen, Yin Cui, Yifan Ding, et al. Cosmos world foundation model platform for physical ai. *arXiv preprint arXiv:2501.03575*, 2025. [2](#), [3](#)
- [2] Mohammad Asim, Christopher Wewer, Thomas Wimmer, Bernt Schiele, and Jan Eric Lenssen. MEt3R: Measuring multi-view consistency in generated images. In *CVPR*, pages 6034–6044, 2025. [1](#), [2](#), [3](#), [6](#), [7](#), [8](#)
- [3] Arpit Bansal, Hong-Min Chu, Avi Schwarzschild, Soumyadip Sengupta, Micah Goldblum, Jonas Geiping, and Tom Goldstein. Universal guidance for diffusion models. In *CVPRW*, pages 843–852, 2023. [3](#), [5](#)
- [4] Shariq Farooq Bhat, Reiner Birk, Diana Wofk, Peter Wonka, and Matthias Müller. ZoeDepth: Zero-shot transfer by combining relative and metric depth. *arXiv preprint arXiv:2302.12288*, 2023. [3](#)
- [5] Tim Brooks, Bill Peebles, Connor Holmes, Will DePue, Yufei Guo, Li Jing, David Schnurr, Joe Taylor, Troy Luhman, Eric Luhman, Clarence Ng, Ricky Wang, and Aditya Ramesh. Video generation models as world simulators, 2024. OpenAI technical report. [6](#)
- [6] Mathilde Caron, Hugo Touvron, Ishan Misra, Herv'e J'egou, Julien Mairal, Piotr Bojanowski, and Armand Joulin. Emerging properties in self-supervised vision transformers. *2021 IEEE/CVF International Conference on Computer Vision (ICCV)*, pages 9630–9640, 2021. [2](#), [3](#)
- [7] Subhabrata Choudhury, Laurynas Karazija, Iro Laina, Andrea Vedaldi, and Christian Rupprecht. Guess what moves: Unsupervised video and image segmentation by anticipating motion. In *BMVC*, 2022. [3](#)
- [8] Angela Dai, Angel X. Chang, Manolis Savva, Maciej Halber, Thomas Funkhouser, and Matthias Nießner. ScanNet: Richly-annotated 3D reconstructions of indoor scenes. In *CVPR*, 2017. [5](#), [3](#)

[9] Daniel DeTone, Tomasz Malisiewicz, and Andrew Rabinovich. Superpoint: Self-supervised interest point detection and description. *2018 IEEE/CVF Conference on Computer Vision and Pattern Recognition Workshops (CVPRW)*, pages 337–33712, 2017. 3

[10] Haoyi Duan, Hong-Xing Yu, Sirui Chen, Li Fei-Fei, and Jiajun Wu. WorldScore: A unified evaluation benchmark for world generation. In *ICCV*, 2025. 1, 2, 3

[11] Daniel Geng and Andrew Owens. Motion guidance: Diffusion-based image editing with differentiable motion estimators. In *ICLR*, 2024. 3

[12] Google DeepMind. Veo: a text-to-video generation system. Technical report, 2025. Veo 3 technical report. 6

[13] Yoav HaCohen, Nisan Chiprut, Benny Brazowski, Daniel Shalem, Dudu Moshe, Eitan Richardson, Eran Levin, Guy Shiran, Nir Zabari, Ori Gordon, Poriya Panet, Sapir Weissbuch, Victor Kulikov, Yaki Bitterman, Zeev Melumian, and Ofir Bibi. LTX-Video: Realtime video latent diffusion. *arXiv preprint arXiv:2501.00103*, 2024. 6

[14] Xinran Han, Todd Zickler, and Ko Nishino. Multistable shape from shading emerges from patch diffusion. *NeurIPS*, 37:34686–34711, 2024. 3

[15] Richard Hartley and Andrew Zisserman. *Multiple View Geometry in Computer Vision*. Cambridge University Press, 2003. 2, 3

[16] Yutong He, Naoki Murata, Chieh-Hsin Lai, Yuhta Takida, Toshimitsu Uesaka, Dongjun Kim, Wei-Hsiang Liao, Yuki Mitsuji, J. Zico Kolter, Ruslan Salakhutdinov, and Stefano Ermon. Manifold preserving guided diffusion. In *ICLR*, 2024. 5

[17] Wenyi Hong, Ming Ding, Wendi Zheng, Xinghan Liu, and Jie Tang. CogVideo: Large-scale pretraining for text-to-video generation via transformers. *arXiv preprint arXiv:2205.15868*, 2022. 6

[18] Chun-Hao Paul Huang, Niloy Mitra, Hyeyonho Jeong, Jae Shin Yoon, and Duygu Ceylan. JOG3R: Towards 3D-consistent video generators. In *BMVC*, 2025. 3

[19] Nan Huang, Wenzhao Zheng, Chenfeng Xu, Kurt Keutzer, Shanghang Zhang, Angjoo Kanazawa, and Qianqian Wang. Segment any motion in videos. In *CVPR*, pages 3406–3416, 2025. 3, 1

[20] Ziqi Huang, Yinan He, Jiashuo Yu, Fan Zhang, Chenyang Si, Yuming Jiang, Yuanhan Zhang, Tianxing Wu, Qingyang Jin, Nattapol Chanpaisit, Yaohui Wang, Xinyuan Chen, Limin Wang, Dahua Lin, Yu Qiao, and Ziwei Liu. VBench: Comprehensive benchmark suite for video generative models. *CVPR*, pages 21807–21818, 2023. 2, 3, 6

[21] Ziqi Huang, Fan Zhang, Xiaoje Xu, Yinan He, Jiashuo Yu, Ziyue Dong, Qianli Ma, Nattapol Chanpaisit, Chenyang Si, Yuming Jiang, Yaohui Wang, Xinyuan Chen, Yingcong Chen, Limin Wang, Dahua Lin, Yu Qiao, and Ziwei Liu. VBench++: Comprehensive and versatile benchmark suite for video generative models. *ArXiv*, 2024. 2, 3, 6

[22] Sang-Sub Jang, Taekyung Ki, Jaehyeong Jo, Jaehong Yoon, Soo Ye Kim, Zhe L. Lin, and Sung Ju Hwang. Frame guidance: Training-free guidance for frame-level control in video diffusion models. *ArXiv*, abs/2506.07177, 2025. 3, 5

[23] Weijie Kong, Qi Tian, Zijian Zhang, Rox Min, Zuozhuo Dai, Jin Zhou, Jiangfeng Xiong, Xin Li, Bo Wu, Jianwei Zhang, et al. HunyuanVideo: A systematic framework for large video generative models. *arXiv preprint arXiv:2412.03603*, 2024. 6

[24] Hala Lamdouar, Weidi Xie, and Andrew Zisserman. Segmenting invisible moving objects. *BMVC*, 2021. 3

[25] Philipp Lindenberger, Paul-Edouard Sarlin, and Marc Pollefeys. Lightglue: Local feature matching at light speed. *2023 IEEE/CVF International Conference on Computer Vision (ICCV)*, pages 17581–17592, 2023. 3

[26] Yaofang Liu, Xiaodong Cun, Xuebo Liu, Xintao Wang, Yong Zhang, Haoxin Chen, Yang Liu, Tieyong Zeng, Raymond H. Chan, and Ying Shan. EvalCrafter: Benchmarking and evaluating large video generation models. *CVPR*, pages 22139–22149, 2023. 5

[27] David G. Lowe. Object recognition from local scale-invariant features. *Proceedings of the Seventh IEEE International Conference on Computer Vision*, 2:1150–1157 vol.2, 1999. 3

[28] Andreas Lugmayr, Martin Danelljan, Andrés Romero, Fisher Yu, Radu Timofte, and Luc Van Gool. RePaint: Inpainting using denoising diffusion probabilistic models. *CVPR*, pages 11451–11461, 2022. 5

[29] Hyelin Nam, Jaemin Kim, Dohun Lee, and Jong Chul Ye. Optical-flow guided prompt optimization for coherent video generation. *CVPR*, pages 7837–7846, 2024. 3

[30] Alec Radford, Jong Wook Kim, Chris Hallacy, Aditya Ramesh, Gabriel Goh, Sandhini Agarwal, Girish Sastry, Amanda Askell, Pamela Mishkin, Jack Clark, Gretchen Krueger, and Ilya Sutskever. Learning transferable visual models from natural language supervision. In *International Conference on Machine Learning*, 2021. 2, 3

[31] Nikhila Ravi, Valentin Gabeur, Yuan-Ting Hu, Ronghang Hu, Chaitanya Ryali, Tengyu Ma, Haitham Khedr, Roman Rädle, Chloe Rolland, Laura Gustafson, Eric Mintun, Junting Pan, Kalyan Vasudev Alwala, Nicolas Carion, Chao-Yuan Wu, Ross Girshick, Piotr Dollár, and Christoph Feichtenhofer. SAM 2: Segment anything in images and videos. *arXiv preprint arXiv:2408.00714*, 2024. 6

[32] Jeremy Reizenstein, Roman Shapovalov, Philipp Henzler, Luca Sbordone, Patrick Labatut, and David Novotny. Common objects in 3D: Large-scale learning and evaluation of real-life 3d category reconstruction. In *ICCV*, 2021. 5, 3

[33] Xuanchi Ren, Tianshang Shen, Jiahui Huang, Huan Ling, Yifan Lu, Merlin Nimier-David, Thomas Müller, Alexander Keller, Sanja Fidler, and Jun Gao. Gen3C: 3D-informed world-consistent video generation with precise camera control. In *CVPR*, pages 6121–6132, 2025. 3

[34] Paul D. Sampson. Fitting conic sections to “very scattered” data: An iterative refinement of the bookstein algorithm. *Computer graphics and image processing*, 1982. 2, 3

[35] Zachary Teed and Jia Deng. DROID-SLAM: Deep visual slam for monocular, stereo, and RGB-D cameras. *NeurIPS*, 34:16558–16569, 2021. 3

[36] Team Wan, Ang Wang, Baole Ai, Bin Wen, Chaojie Mao, Chen-Wei Xie, Di Chen, Feiwei Yu, Haiming Zhao, Jianxiao Yang, et al. Wan: Open and advanced large-scale video

generative models. *arXiv preprint arXiv:2503.20314*, 2025.

6

- [37] Jianyuan Wang, Minghao Chen, Nikita Karaev, Andrea Vedaldi, Christian Rupprecht, and David Novotny. VGGT: Visual geometry grounded transformer. In *CVPR*, 2025. 3, 4, 5
- [38] Shuzhe Wang, Vincent Leroy, Yohann Cabon, Boris Chidlovskii, and Jerome Revaud. DUSt3R: Geometric 3D vision made easy. In *CVPR*, pages 20697–20709, 2024. 3
- [39] Yinhui Wang, Jiwen Yu, and Jian Zhang. Zero-shot image restoration using denoising diffusion null-space model. In *ICLR*, 2023. 5
- [40] Junyu Xie, Weidi Xie, and Andrew Zisserman. Segmenting moving objects via an object-centric layered representation. *NeurIPS*, 35:28023–28036, 2022. 3
- [41] Junyu Xie, Charig Yang, Weidi Xie, and Andrew Zisserman. Moving object segmentation: All you need is sam (and flow). In *ACCV*, pages 162–178, 2024.
- [42] Charig Yang, Hala Lamdouar, Erika Lu, Andrew Zisserman, and Weidi Xie. Self-supervised video object segmentation by motion grouping. In *ICCV*, pages 7177–7188, 2021. 3
- [43] Lihe Yang, Bingyi Kang, Zilong Huang, Zhen Zhao, Xiaogang Xu, Jiashi Feng, and Hengshuang Zhao. Depth anything V2. *NeurIPS*, 37:21875–21911, 2024. 3
- [44] Zhuoyi Yang, Jiayan Teng, Wendi Zheng, Ming Ding, Shiyu Huang, Jiazheng Xu, Yuanming Yang, Wenyi Hong, Xiaohan Zhang, Guanyu Feng, et al. CogVideoX: Text-to-video diffusion models with an expert transformer. *arXiv preprint arXiv:2408.06072*, 2024. 5, 6
- [45] Chandan Yeshwanth, Yueh-Cheng Liu, Matthias Nießner, and Angela Dai. ScanNet++: A high-fidelity dataset of 3D indoor scenes. In *ICCV*, 2023. 5, 3
- [46] Jason J. Yu, Fereshteh Forghani, Konstantinos G. Derpanis, and Marcus A. Brubaker. Long-term photometric consistent novel view synthesis with diffusion models. In *ICCV*, 2023. 2, 3
- [47] Lvmin Zhang, Anyi Rao, and Maneesh Agrawala. Adding conditional control to text-to-image diffusion models. In *ICCV*, pages 3836–3847, 2023. 3
- [48] Qihang Zhang, Shuangfei Zhai, Miguel Angel Bautista Martin, Kevin Miao, Alexander Toshev, Joshua Susskind, and Jiatao Gu. World-consistent video diffusion with explicit 3D modeling. In *CVPR*, pages 21685–21695, 2025. 3
- [49] Yabo Zhang, Yuxiang Wei, Dongsheng Jiang, XIAOPENG ZHANG, Wangmeng Zuo, and Qi Tian. ControlVideo: Training-free controllable text-to-video generation. In *ICLR*, 2024. 3
- [50] Yuchen Zhang, Nikhil Keetha, Chenwei Lyu, Bhuvan Jhamb, Yutian Chen, Yuheng Qiu, Jay Karhade, Shreyas Jha, Yaoyu Hu, Deva Ramanan, Sebastian Scherer, and Wenshan Wang. UFM: A simple path towards unified dense correspondence with flow. In *arXiv*, 2025. 3, 4, 5

GeCo: A Differentiable Geometric Consistency Metric for Video Generation

Supplementary Material

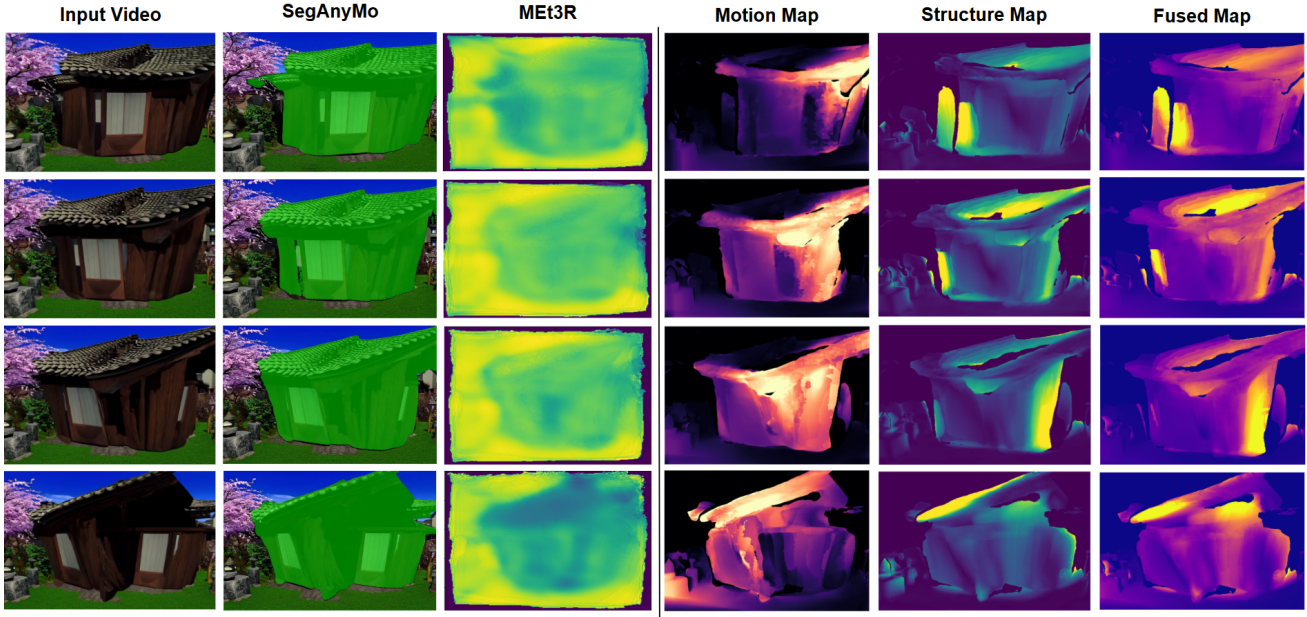


Figure A. **Qualitative comparison on deformation artifacts.** SegAnyMo [19] fails to predict localized motion, while MEt3R [2] produces a blurred score map without region-level detail. In contrast, our method, GeCo, produces interpretable inconsistency maps that precisely highlight subtle, localized geometric distortions rather than masking entire objects.

This supplementary material provides additional qualitative results and comprehensive technical details to support the findings in the main paper. We provide additional visual results (Sec. A), implementation details on geometric consistency calculations and WarpBench construction (Sec. B), hyperparameters for our training-free guidance experiments (Sec. C), and details on our GeCo-Eval benchmark (Sec. D) with the list of text prompts for evaluation (Sec. E).

Please refer to our project webpage for more video visualizations: <https://GeCo-GeoConsistency.github.io>.

A. More Qualitative Results

A.1. Interpretability Comparison

Qualitative comparisons in Fig. A highlight the utility of our metric as a diagnostic tool. While baselines such as MEt3R [2] produce blurred, non-specific score maps, GeCo generates precise maps that isolate specific geometric distortions, offering actionable feedback on model performance. Conventional motion-segmentation methods (*e.g.* SegAnyMo [19]) highlight the whole object area as deformation, showing ineffectiveness as a metric.

A.2. Results on GeCo Validation Experiment

We analyze the complementary nature of our motion and structure cues in Fig. B and Fig. C. While the motion cue is essential for detecting surface deformations where depth remains consistent (Fig. B), it often fails during sudden object appearances, misclassifying them as occlusions. In these latter cases, the structure cue proves critical, successfully identifying the hallucinated geometry that the motion cue ignores (Fig. C).

A.3. Results on Guidance Experiment

We provide an extended visual comparison of video generation quality in Fig. E. As shown in the figure, models employing GeCo guidance consistently maintain structural rigidity across complex motions, whereas the baselines exhibit noticeable deformation artifacts.

To further validate the geometric consistency of our generations, we perform 3D reconstruction on the generated clips. As illustrated in Fig. D, videos generated with our guidance yield coherent point clouds, while baseline methods lead to reconstruction failures (*e.g.*, object drift or fracturing) due to temporal inconsistencies.

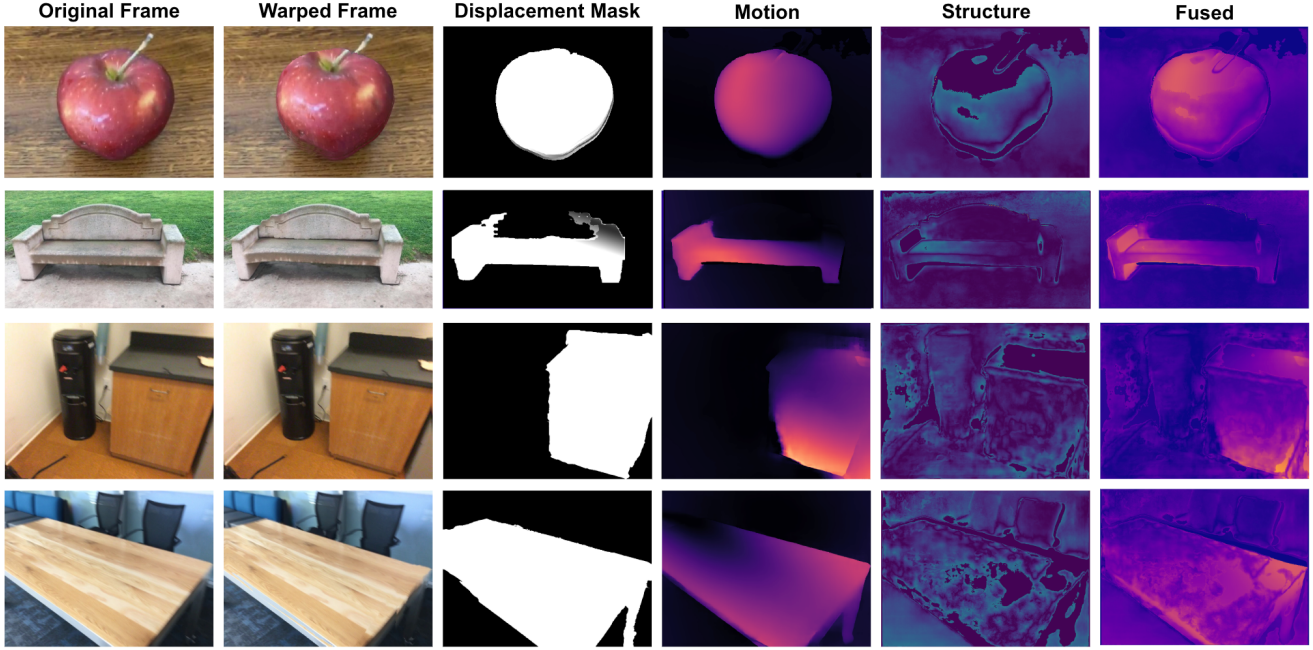


Figure B. **Motion cue validation on WarpBench.** Top two rows: examples from CO3D-Warp; Bottom two rows: examples from ScanNet-Warp. In all examples, the motion map accurately highlights the deformation region (aligning with the displacement mask). In contrast, the structure cue remains insensitive to these surface-level deformations, as they induce only negligible depth variations.

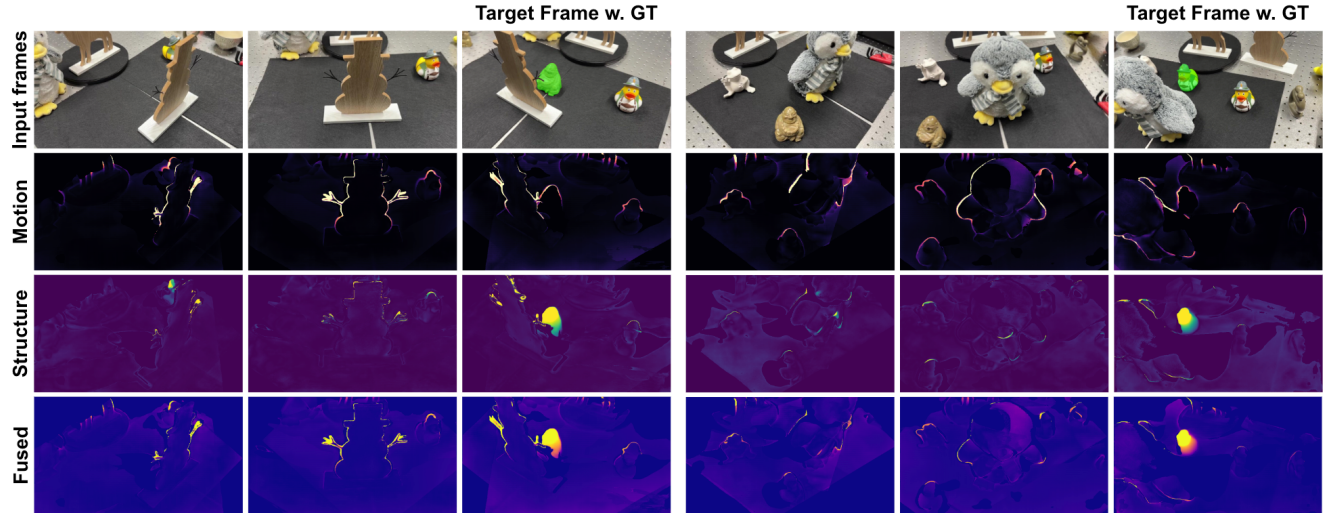


Figure C. **Structure cue validation on OccluBench.** We visualize two examples where objects appear abruptly in the target frame (Left: a statue; Right: a rubber duck). The structure map successfully highlights these inconsistencies. Conversely, the motion cue fails to capture these artifacts, as it classifies the appearing objects as occluded regions and consequently ignores the error region.

B. Implementation Details

B.1. Details on Structure Consistency

In the main paper, we conceptualized structure consistency as the residual between the predicted depth and the reprojected depth map. In our implementation, we compute this

using an inverse warping mechanism to ensure differentiability and sub-pixel accuracy via bilinear sampling.

Let \mathbf{D}_c and \mathbf{D}_i be the depth maps for the current (source) and reference (target) frames, respectively. For a pixel \mathbf{p} in the current frame coordinate system with depth $z_c = \mathbf{D}_c(\mathbf{p})$, we back-project it to a 3D point \mathbf{X} and project it



Figure D. **Impact of GeCo guidance on reconstruction quality.** We observe that GeCo significantly reduces geometric artifacts compared to the baseline. Top: The baseline generates a sink that drifts over time (unnatural motion), leading to misalignment in the 3D reconstruction. Bottom: The baseline suffers from structural deformation, causing the car’s side skirt to fracture into two disjoint segments.

onto the frame of \mathbf{I}_i :

$$\mathbf{p}' = \mathbf{K}_i(\mathbf{R}_{c \rightarrow i}\mathbf{K}_c^{-1}\tilde{\mathbf{p}}z_c + \mathbf{t}_{c \rightarrow i}), \quad (10)$$

where $\tilde{\mathbf{p}}$ is the homogeneous coordinate of \mathbf{p} . Let z_{proj} be the z-coordinate of the point in the reference frame (the predicted distance to the camera).

We sample the reference depth map at the projected location \mathbf{p}' using bilinear interpolation to obtain $\hat{d}_i = \mathbf{D}_i(\mathbf{p}')$. The structure consistency error at pixel \mathbf{p} is computed as the normalized relative depth difference:

$$\mathcal{L}_{\text{geo}}(\mathbf{p}) = \frac{|\hat{d}_i - z_{\text{proj}}|}{z_c}. \quad (11)$$

Occlusion Handling. Instead of explicit z-buffering, we employ a bi-directional geometric consistency check to generate a validity mask \mathbf{M}_{vis} . A pixel \mathbf{p} is considered valid (co-visible) only if it satisfies the forward visibility check:

$$\frac{z_{\text{proj}} - \hat{d}_i}{z_{\text{proj}}} < \tau, \quad (12)$$

where τ is a relative threshold (set to 0.02 in experiments). This filters out pixels where the source point is occluded by a closer surface in the target view. We further refine this mask by performing the inverse check (projecting from i to c) and retaining only the intersection of valid regions.

B.2. Details on Thin-plate-spline for WarpBench

As described in Sec. 4.1 in the main paper, we develop WarpBench based on two open-source datasets: CO3D [32] (*CO3D-Warp*) with object-centric clips and ScanNet++ [8, 45] (*ScanNet-Warp*) with indoor scenes clips. In total, WARBENCH contains 100 object-centric clips (2,000 frames) and 100 scene-level clips (2,000 frames), spanning 50 object categories and 6 indoor environments.

To simulate deformation artifacts, we inject temporally smooth non-rigid warps parameterized by thin-plate splines (TPS), as shown in Fig. 3 in the main paper. For each clip, we sample K control points c_i within the foreground mask via farthest-point sampling (FPS) to ensure coverage. Their 2D displacements $\mathbf{u}_{i,t} \in \mathbb{R}^2$ evolve under a simple temporal model. At each frame t , we fit a TPS warp that maps fixed



Figure E. **Extended visual comparison.** Videos generated with GeCo guidance consistently exhibit fewer deformation artifacts across diverse scenarios.

control points c_i to targets $y_{i,t}$:

$$y_{i,t} = c_i + \mathbf{u}_{i,t}. \quad (13)$$

Specifically, we model the warp as an affine-plus-RBF mapping $f_t : \mathbb{R}^2 \rightarrow \mathbb{R}^2$ with a TPS basis $\phi(r) = r^2 \log r$. The mapping is defined as:

$$f_t(x) = A_t x + a_t + \sum_{i=1}^K w_{i,t} \phi(\|x - c_i\|), \quad (14)$$

where $A_t \in \mathbb{R}^{2 \times 2}$, $a_t \in \mathbb{R}^2$, and $w_{i,t} \in \mathbb{R}^2$ are the TPS parameters. The dense forward displacement $U_t(p)$ at pixel p is derived by:

$$U_t(p) = f_t(p) - p. \quad (15)$$

We localize the deformation with a feathered weight map $w(p) \in [0, 1]$ to calculate $\tilde{U}_t(p)$, and subsequently enforce temporal smoothness via an exponential moving average $\bar{U}_t(p)$:

$$\tilde{U}_t(p) = w(p) U_t(p), \quad (16)$$

$$\bar{U}_t(p) = \beta \bar{U}_{t-1}(p) + (1 - \beta) \tilde{U}_t(p). \quad (17)$$

The final warped frame is obtained by differentiable backward sampling:

$$I_t^{\text{def}}(p) = I_t(p + \bar{U}_t(p)). \quad (18)$$

For every warped frame, we release the dense displacement field $\bar{U}_t(p) \in \mathbb{R}^2$ as ground truth, along with its magnitude $M_t(p)$ when a scalar target is needed:

$$M_t(p) = \|\bar{U}_t(p)\|_2. \quad (19)$$

B.3. Spearman’s Rank Correlation Coefficient

In the deformation localization experiment of WarpBench, we used Spearman’s rank correlation coefficient (SRCC) to measure rank correlation with the ground truth deformation magnitude, here we provide a detailed explanation of this metric: SRCC is a non-parametric measure of rank correlation that evaluates the strength and direction of a monotonic relationship between two ranked variables, defined as $\rho = 1 - \frac{6 \sum d_i^2}{n(n^2-1)}$, where d_i is the difference between the ranks of paired observations and n is the number of pairs.

C. Hyperparameters for Training-free Guidance Experiment

We conduct our experiments using the CogVideoX-5B text-to-video model as the base generator. All inference is performed using `bfloat16` precision on a single NVIDIA H200 GPU. The generated videos consist of $N = 49$ frames with a resolution consistent with the standard model output.

C.1. GeCo Guidance Configuration

To compute the geometric consistency loss \mathcal{L}_{geo} , we utilize two frozen pretrained backbones: VGGT-1B [37] for depth and camera estimation, and UFM-Base [50] for optical flow.

To ensure computational efficiency, we do not decode the full sequence for every gradient update. Instead, we apply Latent Slicing [22] on a fixed set of anchor frames, specifically indices $\mathcal{I} = \{12, 24, 36, 48\}$ (1-based indexing). The residual motion metric is computed in *adjacent* pair mode ($k \rightarrow k + 1$) across these frames. To further accelerate the pipeline, input frames passed to the flow network are down-scaled by a factor of 0.5.

C.2. Sampling and Optimization Schedule

We utilize a standard DDIM sampling trajectory with $T = 50$ inference steps and a Classifier-Free Guidance (CFG) scale of 6.0.

Following the optimization strategy proposed in [22], we apply a recursive denoising schedule where the number of gradient updates R_t varies per timestep t . We utilize a constant step size (learning rate) of $\eta = 3.0$ for all updates. The schedule is divided into three distinct phases:

1. Warm-up ($t \in [0, 2]$): We perform no gradient updates ($R_t = 0$) in the initial steps to establish the global layout.
2. Strong Guidance ($t \in [3, 19]$): We apply $R_t = 3$ updates per step to enforce strong geometric constraints during the formation of structural content.
3. Refinement ($t \in [20, 49]$): We reduce the frequency to $R_t = 2$ updates per step to maintain consistency without disrupting fine texture generation.

To mitigate the accumulation of errors and prevent the latent from drifting off the data manifold during aggressive updates, we strictly employ Time-Travel [16] within the specific interval $t \in [15, 20]$.

D. Details on GeCo-Eval Benchmark

D.1. Prompts Design

As described in Sec. 5.1 in the main paper, we design the benchmark to include four scenarios: (i) object-centric scenes, (ii) indoor scenes, (iii) outdoor scenes, and (iv) appearance-complex scenes (e.g., characterized by high-frequency patterns, reflections, and thin structures). We show the aggregated summary of the prompts in Table A, and the full list of the prompts in Sec. E.

D.2. Motion Metrics

Models that generate very little motion can appear highly temporally consistent, even when they ignore motion-rich prompts. Prior work therefore uses optical flow to detect near-static generations: *EvalCrafter* [26] defines a Flow-Score as the clip-averaged flow magnitude and a Motion AC-Score by thresholding this value, while

Table A. Composition of the GeCo-Eval benchmark. The benchmark is structured around four evaluation scenarios designed to probe geometric consistency, each tested with both slow and fast camera dynamics.

Evaluation Scenario	Dynamics	Example Scenarios
Object-centric scenes: Maintain rigid, detailed geometry of a single isolated object.	Slow	360° orbit of marble bust; push-in on antique globe; upward tilt on bronze horse statue.
	Fast	Rapid orbit of espresso machine; fast dolly in/out on jeweled pocket watch; inward spiral around stone gargoyle.
Indoor scenes: Preserve coherent room layout and global structure during traversal.	Slow	Grand library aisle dolly; gallery arc around abstract sculpture; server-aisle glide.
	Fast	Office hallway sprint; boiler-room right-angle turns; spiral staircase ascent.
Outdoor scenes: Ensure consistency across expansive environments with layered depth.	Slow	Cloister courtyard traverse; under-bridge arch glide; shipping-container row track.
	Fast	Parking-structure sharp turns; underpass colonnade weave; container maze with two right-angle turns.
Appearance-complex scenes: Test fine patterns, reflections, refractions, and dense edges prone to artifacts.	Slow	Chrome motorcycle orbit (stable reflections); glass-brick refraction dolly; mosaic floor lateral slide.
	Fast	Mirror-room orbit; fast lateral across venetian blinds; weave through beaded glass curtains.

VBench/VBench++ [20, 21] report a Dynamic Degree based on whether the largest 5% of per-frame flow magnitudes exceed a threshold. These metrics, however, are not normalized for resolution/FPS and are largely threshold-based, making cross-model comparison difficult when generation settings differ.

Hence, we use a continuous motion statistic with resolution/FPS normalized. Given frames I_t ($t \in \{1, \dots, T\}$), we estimate the optical flow $F_t(x, y)$ and its magnitude $M_t(x, y)$ between I_t and I_{t+1} :

$$F_t(x, y) = (u_t, v_t), \quad (20)$$

$$M_t(x, y) = \sqrt{u_t^2 + v_t^2}. \quad (21)$$

Let W, H be the image width and height. We normalize motion relative to the image diagonal $D = \sqrt{W^2 + H^2}$. After masking invalid pixels, we compute the per-pair normalized displacement m_t :

$$m_t = \text{mean}_{x,y} \left[\frac{M_t(x, y)}{D} \right]. \quad (22)$$

Finally, for a clip of duration S seconds, we define the Total Motion (TM) and Motion Intensity (MI) as:

$$\text{TM} = \sum_{t=1}^{T-1} m_t, \quad (23)$$

$$\text{MI} = \frac{\text{TM}}{S}. \quad (24)$$

Here, TM is a dimensionless measure (fraction of the image diagonal) representing the total path length, which is approximately invariant to FPS for a fixed S . MI represents the corresponding average motion per second. In GeCo-Eval (Tab. 4 in the main paper), we report per-model, per-scenario means and standard deviations of TM and MI, allowing us to interpret geometric consistency jointly with the magnitude of motion produced by the model.

E. List of Text Prompt

E.1. Object-Centric Prompts

E.1.1. Slow camera movements

a1. In a serene gallery, a slow, deliberate 360-degree orbit captures a masterfully carved marble bust, poised elegantly on a polished pedestal. The bust, depicting a serene figure with intricate details, remains perfectly centered as the camera glides smoothly around it. The lighting casts soft shadows, accentuating the delicate features and the smooth texture of the marble. The exposure and white balance are meticulously set, ensuring the bust's timeless beauty is captured in pristine clarity. The focus remains sharp, highlighting every curve and chisel mark, while the background fades into a gentle blur, emphasizing the sculpture's artistry. The only motion is the camera's graceful orbit, creating a mesmerizing, uninterrupted view of this exquisite masterpiece.

a2. The camera gracefully advances toward an exquisite antique globe perched on an intricately carved wooden stand, its surface illuminated by soft, ambient light. As the frame narrows, the globe's aged paper grain becomes evident, showcasing faded cartographic details and muted colors that whisper tales of exploration. The brass meridian, polished yet timeworn, gleams subtly, its engraved lines and numbers hinting at a bygone era of navigation. The room is enveloped in a serene stillness, with no hint of wind or vibration, allowing the globe's historical elegance to captivate the viewer. The camera's gentle motion is the only dynamic element, drawing the eye closer to the globe's timeless allure.

a3. The video begins with a close-up of the bronze horse statue's hooves, capturing the intricate details of the sculpted muscles and the polished sheen of the metal. As the camera tilts upward at a steady, deliberate pace, the viewer is drawn into the artistry of the statue, revealing the powerful legs and the graceful curve of the horse's body. The room remains still and silent, with soft, even lighting casting gentle shadows that accentuate the statue's form. The focus remains sharp, highlighting the texture and craftsmanship of the bronze. The camera continues its ascent, passing the horse's strong neck, until it reaches the noble head, capturing the lifelike expression and finely detailed features, completing the serene and contemplative journey.

a4. A meticulously crafted lateral dolly shot begins at the platen of a vintage typewriter, its textured roller and paper guide evoking a sense of nostalgia. The camera glides smoothly, revealing the intricate array of keys, each with its own unique patina, hinting at countless stories typed over the years. The levers and typebars, though stationary, suggest potential energy, poised for action. As the camera continues its journey, the focus shifts to the side panel, showcasing the elegant curves and mechanical artistry of the typewriter's design. The entire scene is bathed in soft, ambient light, highlighting the timeless beauty of this classic writing instrument.

a5. The camera begins its graceful descent from a bird's-eye view, revealing a stunning ceramic vase with intricate glazed relief patterns. As it slowly lowers, the vase's exquisite details become more pronounced, showcasing delicate floral motifs and swirling designs in rich, earthy tones. The vase sits on a polished wooden surface, its glossy finish reflecting the soft ambient light. The surroundings remain perfectly still, enhancing the vase's elegance and craftsmanship. The camera continues its descent, eventually settling into a tight side profile, capturing the vase's curves and textures with precision. The lighting remains constant, casting gentle shadows that accentuate the vase's artistry, creating a serene and contemplative visual experience.

a6. The camera gracefully arcs around a luxurious gilded wall mirror, its ornate frame glistening with intricate golden details. The mirror reflects a serene, softly lit room, capturing only the immediate backdrop—a plush velvet armchair and a delicate vase of fresh lilies on a polished wooden table. The camera maintains a consistent distance, ensuring the reflections remain steady and undisturbed. The room's ambiance is tranquil, with warm, ambient lighting casting gentle shadows. The mirror's surface is pristine, reflecting the elegance of the setting without any flicker or change, as the camera's smooth motion reveals the timeless beauty of the scene.

a7. The camera begins its slow, deliberate journey at the base of a towering wooden abstract sculpture, its intricate grain and texture immediately captivating. As the dolly glides diagonally upward, the sculpture's complex curves and angles are revealed, each facet catching the ambient light in a unique way, creating a play of shadows and highlights. The fixed focus ensures every detail remains sharp, while the consistent white balance maintains the sculpture's natural hues. The background remains unobtrusive, allowing the sculpture's artistry to dominate the frame. The camera's smooth ascent culminates at the sculpture's opposite top corner, offering a final, breathtaking perspective of this wooden masterpiece.

a8. The camera glides smoothly in a precise orbit around an ancient stone relief wall panel, capturing the intricate artistry of the chiseled figures. As it moves laterally, the depth of each groove and the play of light and shadow in the recessed areas become more pronounced, revealing the skill of the artisans. The relief, depicting a serene scene of historical significance, remains perfectly still, allowing the viewer to appreciate the fine details and textures. The environment, a dimly lit gallery with soft ambient lighting, enhances the timeless quality of the stone, while the camera's path is the sole source of motion,

creating a dynamic yet tranquil viewing experience.

a9. A luxurious mechanical pocket watch rests open on deep crimson velvet, its intricate details captured in stunning macro. The camera begins its slow, deliberate pan at the ornate crown, highlighting the delicate engravings and polished metal. As the lens glides smoothly across the watch's surface, the frozen hands and gears are revealed, each component meticulously crafted and gleaming under the soft, focused illumination. The journey continues to the escapement, where the precision of the jewel settings is showcased, their vibrant colors contrasting beautifully with the metallic intricacies. The entire scene exudes timeless elegance, with the velvet's rich texture enhancing the watch's exquisite craftsmanship.

a10. The camera gracefully orbits a meticulously crafted bonsai tree, positioned on a low, elegant stand, capturing the intricate details of its textured bark and the delicate wirework shaping its branches. The lens remains at leaf height, offering an intimate view of the bonsai's artistry, with each leaf and branch in sharp focus. The serene atmosphere is undisturbed by any breeze, ensuring the leaves remain perfectly still, enhancing the tranquility of the scene. The exposure is expertly balanced, highlighting the rich hues of the bonsai's foliage and the subtle variations in its bark. The camera's smooth, continuous motion is the sole dynamic element, creating a mesmerizing visual experience.

E.1.2. Fast camera movements

a11. The camera swiftly orbits a gleaming, polished metal espresso machine, capturing its sleek, reflective surface in stunning detail. As it circles, the machine's curves and edges reveal dazzling specular highlights, creating a dynamic play of light and shadow. The environment remains perfectly still, with the espresso machine standing as the centerpiece against a minimalist backdrop. The lighting is expertly set, casting soft, even illumination that accentuates the machine's contours. The camera's rapid movement provides a seamless 360-degree view, showcasing the espresso machine's elegant design and craftsmanship from every angle, while the surroundings remain unchanged.

a12. The video begins with a swift dolly-in towards an exquisite, vintage pocket watch, its surface adorned with intricate jewels that catch the light. As the camera zooms in, the focus sharpens on the delicate, engraved monogram, revealing the initials "J.L." in elegant script. The watch's face, a masterpiece of craftsmanship, is frozen in time, its hands paused at precisely 10:10. The exposure remains constant, highlighting the watch's gleaming metallic finish and the sparkle of its jewels. Suddenly, the camera rapidly pulls back, revealing the full grandeur of the pocket watch, resting on a plush velvet surface, its timeless elegance captured in perfect clarity.

a13. The video begins with a close-up of the base of a grand, fluted stone column, its intricate grooves and textures highlighted by steady, soft lighting. The camera swiftly tilts upward, maintaining perfect alignment with the column's vertical lines, revealing the elegant, timeless craftsmanship of the stonework. As the camera ascends, the column's fluting creates a mesmerizing pattern, leading the viewer's eye toward the capital. Upon reaching the top, the capital is revealed in all its ornate glory, adorned with classical acanthus leaves and scrolls, set against the backdrop of a stately, immobile room. The entire scene remains serene and unchanging, with the brisk camera movement providing the only sense of motion.

a14. A sleek, dynamic arc swiftly encircles a vintage film camera perched on a sturdy tripod, capturing its essence from a front three-quarter angle to a rear three-quarter perspective. The camera, a classic piece with intricate dials and a polished lens, remains perfectly still, exuding timeless elegance. The tripod, robust and unwavering, supports the camera with precision. As the viewpoint sweeps rapidly around, maintaining a constant height, the background blurs into a soft focus, emphasizing the camera's intricate details and craftsmanship. The lighting casts subtle highlights on the camera's metallic surface, enhancing its vintage allure.

a15. A sleek, dynamic shot captures a rapid lateral pass across a classic wooden chessboard, where two rooks stand as sentinels at opposite ends. The camera glides swiftly, skimming just above the meticulously arranged pieces, each casting a sharp shadow on the polished squares. The board's plane remains nearly parallel to the sensor, creating a mesmerizing blur of alternating dark and light squares. The pieces, carved with precision, stand immobile and unwavering, their intricate details highlighted by steady, soft lighting. The focus remains sharp, emphasizing the rooks' commanding presence, while the camera's swift motion creates a sense of urgency and fluidity.

a16. The camera swiftly ascends from a polished wooden tabletop, capturing the elegant rise towards a crystal decanter, its intricate facets glistening under soft, ambient lighting. The room, adorned with rich mahogany furniture and subtle, warm tones, remains perfectly still, exuding an air of timeless sophistication. As the camera reaches its zenith, the decanter's pristine surface reflects the light in a steady, mesmerizing dance of highlights, maintaining a serene, unwavering brilliance. The final top-down view reveals the decanter's symmetrical beauty, its contents a deep amber, contrasting with the room's muted elegance, creating a harmonious visual symphony.

a17. The camera swiftly pans across a meticulously arranged row of antique bottles, each uniquely shaped and colored, their glass surfaces reflecting a warm, ambient light. As the camera moves, the labels blur into a kaleidoscope of vintage typography and faded hues. Suddenly, the motion halts with precision on the central bottle, its label featuring ornate script and

intricate detailing, capturing the essence of a bygone era. The camera lingers momentarily, allowing the viewer to absorb the craftsmanship and history encapsulated in the label. Then, with a seamless transition, the camera resumes its rapid journey, leaving the bottles in a serene, undisturbed stillness.

a18. The camera begins its journey with a swift upward motion, revealing a vintage tabletop gramophone in exquisite detail. As it ascends, the polished wooden base and intricate brass horn come into view, capturing the essence of a bygone era. The camera then gracefully arcs over the gramophone, offering a bird's-eye perspective of the stationary needle poised above the silent vinyl record. The lighting casts gentle shadows, enhancing the gramophone's timeless elegance. As the camera descends on the opposite side, it focuses on the record's grooves, capturing the texture and craftsmanship. The scene concludes with the camera at platter height, emphasizing the gramophone's silent anticipation, as if waiting for the music to begin.

a19. The camera swiftly zig-zags towards a charming, intricately detailed miniature dollhouse, capturing its quaint architecture and tiny furnishings in high definition. The first quick step reveals the dollhouse's vibrant exterior, with its pastel colors and delicate window frames, while the second step shifts the perspective, offering a closer view of the meticulously arranged furniture inside, including a tiny wooden table and chairs. Throughout the sequence, the horizon remains perfectly level, emphasizing the dynamic movement of the camera against the stillness of the scene. The absence of any breeze or motion within the dollhouse enhances the contrast between the camera's rapid approach and the serene, static environment.

a20. The camera begins its journey with a sweeping motion around a majestic stone gargoyle perched atop an ancient cathedral, its intricate details illuminated by the soft glow of twilight. As the camera spirals inward, the gargoyle's menacing features, including its sharp fangs and piercing eyes, become more pronounced against the backdrop of the dusky sky. The spiral tightens smoothly, revealing the texture of the weathered stone, capturing every crack and crevice with precision. The background remains a constant, blurred tapestry of gothic architecture, while the exposure and focus remain locked, ensuring the gargoyle's fierce expression is the focal point. The spiral concludes with a tight profile shot, emphasizing the gargoyle's formidable presence and the artistry of its creation.

E.2. Indoor Prompts

E.2.1. Slow camera movements

b1. The camera glides smoothly down the central aisle of a grand library, flanked by towering bookcases packed tightly with an array of colorful books, their spines creating a mosaic of knowledge. The shelves, lined with neatly arranged volumes, are interspersed with small, elegant signs indicating various genres and sections. The lighting is warm and steady, casting a gentle glow that highlights the rich wood of the bookcases and the intricate patterns of the carpeted floor. As the camera advances at a constant pace, the scene remains perfectly still, evoking a sense of timelessness and tranquility, inviting viewers to immerse themselves in the serene ambiance of this literary sanctuary.

b2. In a serene, minimalist gallery, the camera gracefully arcs around a solitary abstract sculpture, its smooth curves and intricate textures highlighted by the steady, soft lighting. The sculpture, a fusion of metal and stone, stands as the focal point, its form evoking a sense of mystery and contemplation. Glass display cases, housing delicate artifacts, and subtle wall labels linger in the periphery, their presence understated yet integral to the gallery's ambiance. The constant lighting casts gentle shadows, enhancing the sculpture's allure. The only movement is the camera's fluid motion, creating a tranquil, immersive experience that invites reflection and appreciation.

b3. The camera glides smoothly down an opulent hotel corridor, perfectly centered, revealing a symphony of intricate details. Richly patterned carpets stretch endlessly beneath, their designs echoing elegance and sophistication. Ornate sconces cast a warm, steady glow, illuminating the corridor with a timeless ambience. Each door, identical yet unique, stands as a sentinel, adorned with polished brass numbers and gleaming handles. Discreet signage, tastefully placed, guides unseen guests with understated grace. The walls, adorned with subtle textures, frame the scene, while the camera's deliberate, unwavering motion creates a mesmerizing journey through this serene, luxurious passageway.

b4. The camera glides smoothly across a pristine stainless-steel commercial kitchen, capturing the gleaming surfaces of industrial-grade appliances, neatly arranged shelves, and an array of utensils and pans. The countertops, lined with culinary tools, reflect the ambient light, creating a serene, almost clinical atmosphere. As the camera moves parallel to the counters, the symmetry of the kitchen's layout becomes apparent, with each element meticulously organized. The fixed exposure and focus highlight the kitchen's immaculate condition, emphasizing the polished metal and the quiet stillness of the space, devoid of any steam, water, or fan motion, offering a tranquil, undisturbed view.

b5. In a grand museum hall, the camera glides gracefully, capturing the serene ambiance. Display plinths, adorned with intricate artifacts, stand in orderly rows, each accompanied by detailed information placards. The lighting casts a soft, consistent glow, highlighting the exhibits' historical significance. As the camera moves, it reveals the majestic dinosaur

skeleton, its massive feet firmly planted, leading up to its towering skull. The skeletal structure, a testament to ancient times, remains motionless, exuding a sense of timelessness. The camera's steady drift emphasizes the hall's quiet reverence, inviting viewers to immerse themselves in the museum's rich tapestry of history.

b6. The camera glides smoothly along a narrow server aisle, maintaining a precise 1.5-meter height, capturing the dense arrangement of towering server racks. Each cabinet is meticulously organized, with neatly labeled cables running in disciplined lines, creating a sense of order and efficiency. The steady glow of indicator lights on the servers casts a soft, ambient illumination, highlighting the sleek, metallic surfaces of the equipment. The environment is silent and unyielding, exuding a sense of technological precision and control. As the camera moves parallel to the cabinets, the rigid symmetry of the scene is emphasized, offering a glimpse into the heart of a meticulously maintained data center.

b7. The camera smoothly glides down a bustling supermarket aisle, capturing a vibrant array of neatly stacked boxed and canned goods, each adorned with colorful labels and enticing graphics. Price tags dangle from the shelves, offering deals and discounts, while shelf talkers highlight special promotions, all frozen in time. The camera maintains a shallow oblique angle, providing a dynamic perspective that emphasizes the abundance and variety of products. The aisle is brightly lit, casting a warm glow over the scene, as the camera advances steadily, creating a sense of anticipation and discovery amidst the stillness of the packaging and signage.

b8. In a spacious, modern conference room, the camera smoothly glides around a large, polished wooden table, meticulously set for a meeting. The table is surrounded by sleek, ergonomic chairs, each with a notepad and pen neatly placed in front. Crystal-clear water glasses catch the light, casting subtle reflections on the table's surface. Cable grommets are strategically positioned, hinting at the room's technological readiness. The ambient lighting is soft and consistent, creating a professional yet inviting atmosphere. As the camera circles, the scene remains perfectly still, capturing the anticipation of a gathering, with only the camera's gentle motion breaking the serene stillness.

b9. The camera glides slowly through a dimly lit antique shop, revealing a labyrinth of stacked vintage furniture, ornate lamps, and gilded frames. Each shelf overflows with eclectic trinkets, from delicate porcelain figurines to tarnished brass compasses. The air is thick with the scent of aged wood and history, as the camera weaves between narrow aisles, brushing past velvet-upholstered chairs and intricately carved tables. Dust motes dance in the soft, golden light filtering through stained glass windows, casting colorful patterns on the worn wooden floor. The shop remains eerily still, a silent guardian of forgotten stories, as the camera's gentle motion breathes life into the timeless treasures.

b10. The camera smoothly glides through a bustling workshop, revealing a series of workbenches laden with an array of hand tools, neatly organized bins, and pegboards adorned with hanging implements. Parts trays, filled with various components, line the benches, each meticulously arranged. The lighting casts a warm, consistent glow, highlighting the rich textures of wood and metal. The focus remains sharp, capturing every detail of the stationary objects, from the gleaming wrenches to the colorful bins. As the camera tracks parallel to the benches, the scene exudes a sense of order and craftsmanship, with the fixed exposure maintaining a clear, vivid view of this industrious space.

E.2.2. Fast camera movements

b11. The camera races down an endless office hallway, capturing a thrilling high-speed journey. The walls are lined with identical wooden doors, each with polished brass handles, creating a rhythmic pattern. Bright red exit signs hang above every few doors, their glow casting a steady light on the neutral-toned walls. Overhead, fluorescent ceiling fixtures illuminate the path with a consistent, cool white light, casting no shadows. The floor is carpeted in a muted gray, providing a sense of continuity. As the camera zooms forward, the static objects blur slightly at the edges, enhancing the sensation of speed, while maintaining perfect alignment and balance.

b12. The camera glides swiftly through a vast warehouse aisle, flanked by towering pallet racks stacked with neatly arranged cartons, each adorned with vibrant labels. The scene is bathed in soft, ambient lighting, casting gentle shadows on the polished concrete floor. As the camera hugs the centerline, it executes smooth, fluid yaw changes, offering dynamic perspectives of the meticulously organized inventory. The pallets and signage remain perfectly still, creating a striking contrast to the seamless motion of the camera. The journey through the aisle feels like a dance, with the camera's graceful movements highlighting the warehouse's orderly precision and expansive scale.

b13. The camera swiftly navigates through a labyrinthine boiler room, weaving through a dense network of pipes, valves, and gauges. It makes sharp, precise right-angle turns at each junction, capturing the intricate industrial landscape. The scene is bathed in steady, even lighting, highlighting the metallic sheen of the equipment. The walkways are lined with sturdy gratings, and the camera's movement is fluid and rapid, yet the environment remains eerily still, with no vibrations or steam emissions. The constant exposure maintains a clear view of the complex machinery, while the camera's agile dance creates a dynamic visual journey through the mechanical maze.

b14. The camera begins its graceful descent from a grand balcony, capturing the intricate details of the ornate railings and plush, empty seats below. As it swoops downward, the theater's rich red and gold color scheme becomes more pronounced, with rows of seats stretching out like a sea of anticipation. The camera glides past the elegant acoustic panels lining the walls, their design enhancing the theater's opulent atmosphere. The steady, warm glow of the overhead lights bathes the scene in a golden hue, highlighting the theater's grandeur. As the camera approaches the stage, the polished wooden floor of the apron gleams under the lights, inviting the viewer into the heart of this majestic, silent space.

b15. The camera swiftly ascends a sleek, modern spiral staircase in a spacious office atrium, capturing the polished metal handrails and glass balusters in sharp detail. As it spirals upward, the lens brushes past minimalist signage, reflecting the building's contemporary design. The environment remains static and pristine, with the staircase's geometric precision emphasized by the constant radius of the climb. The atrium's ambient lighting casts subtle reflections on the surfaces, enhancing the sense of motion. The camera's ascent is smooth and uninterrupted, offering a dynamic perspective of the architectural elegance and the stillness of the surrounding space.

b16. The camera embarks on a dynamic barrel-roll journey through a luminous glass atrium corridor, where sunlight streams through expansive windows, casting intricate patterns on the polished floor. As the camera gracefully rotates 180 degrees, the corridor's features remain steadfast: sleek planters brimming with verdant foliage, modern benches inviting rest, and sleek directory boards offering guidance. The reflections on the glass walls and floor remain undisturbed, creating a mesmerizing kaleidoscope of light and shadow. The camera's fluid motion captures the essence of the space, transforming the atrium into a captivating dance of architecture and light.

b17. The camera swiftly navigates through a labyrinth of office cubicles, each enclosed by beige partitions, revealing a sea of identical workspaces. Desktops and monitors, displaying static spreadsheets and graphs, line the desks, while cable trays snake overhead, adding to the structured chaos. The camera makes a sharp ninety-degree turn, narrowly avoiding a stack of neatly organized files, before continuing its rapid journey. Another tight turn reveals more cubicles, each identical yet distinct, with personal touches like family photos and coffee mugs. The static screens and still environment contrast with the camera's relentless speed, creating a dynamic visual experience.

b18. The camera swiftly navigates a library's cross-aisle, darting between towering bookshelves densely packed with colorful spines and neatly labeled endcaps. As it races forward, the camera captures the intricate details of book titles and the orderly arrangement of carts and signs, all fixed in place. The lighting remains steady, casting a warm glow over the scene, enhancing the rich textures of the books and the polished wood of the shelves. Suddenly, the camera pivots sharply around a freestanding shelf, revealing a new perspective of the library's labyrinthine layout, before continuing its rapid journey through the quiet, knowledge-filled sanctuary.

b19. The camera swiftly glides through a bustling electronics store aisle, capturing rows of neatly stacked boxed products and sleek demo stations. The shelves are lined with vibrant packaging, showcasing the latest gadgets and devices. As the camera moves, it reveals a variety of electronics, from headphones to smart speakers, all meticulously arranged. The store is filled with the hum of quiet chatter and the soft rustle of packaging. The camera's journey culminates in a dramatic halt at a central display, where a large, prominent screen stands, its surface reflecting the ambient light. Despite the dynamic sweep, all screens remain static, their blank faces contrasting with the lively atmosphere, emphasizing the anticipation of technology yet to be activated.

b20. The camera swiftly descends through a spacious, modern elevator lobby atrium, capturing the sleek design of the space. Rows of metallic mailboxes line the walls, their polished surfaces reflecting the ambient light. Elegant signage, with clear, bold lettering, guides visitors through the area. As the camera glides downward, it passes over a series of sleek, stainless steel turnstiles, their surfaces gleaming under the atrium's soft lighting. The descent continues from the mezzanine rail height, offering a panoramic view of the lobby's architectural details, down to the polished marble floor. The camera advances steadily toward the closed elevator doors, which stand as a focal point. Throughout the descent, the elevator indicators remain steady, their lights unwavering, emphasizing the smooth, uninterrupted motion of the camera's journey.

E.3. Outdoor Prompts

E.3.1. Slow camera movements

c1. The camera glides slowly through a serene cloister courtyard, enveloped by elegant arcades on each side. The stone columns, adorned with intricately carved capitals, stand as silent sentinels beneath the roofline, their artistry captured in exquisite detail. The courtyard's floor is a mosaic of aged stone tiles, each telling its own story. The ambient light bathes the scene in a soft, timeless glow, casting gentle shadows that dance across the surfaces. As the camera advances, the tranquility of the space is palpable, with the arches framing views of the lush, manicured garden at the center, inviting contemplation and peace.

c2. In a narrow, ancient stone alley, the camera glides smoothly, capturing the intricate textures of weathered facades, where every crack and crevice tells a story of time. The alley is flanked by towering stone walls, their surfaces adorned with ornate reliefs and timeworn lintels, each doorway a portal to history. The atmosphere is still and silent, with no breeze to disturb the rigid tranquility. As the camera orbits, it remains close to the walls, emphasizing the craftsmanship and detail of the stonework, while the alley's narrow confines create an intimate, almost claustrophobic ambiance, leaving the distant world unseen and mysterious.

c3. The camera smoothly glides along a row of vibrant shipping containers, stacked three high, their bold colors contrasting against the muted sky. The containers, in shades of red, blue, and green, stand in perfect alignment, their surfaces weathered by time and travel. The yard is enclosed by a sturdy chain-link fence, its metallic sheen catching the light, while the tops of the containers remain just below the frame's upper edge, creating a sense of containment and order. The scene is still and silent, with no movement or fluttering fabric, emphasizing the solitude and industrial beauty of the setting as the camera tracks steadily along the row.

c4. The camera glides smoothly beneath a series of massive concrete bridge arches, capturing the intricate details of the structure. Each arch, with its weathered surface and subtle variations in texture, stands as a testament to engineering prowess. The camera moves gracefully from one pier to the next, maintaining a steady path under the deck, revealing the symmetry and strength of the construction. The surrounding environment is serene, with the gentle sound of water echoing softly. Light filters through the gaps, casting dynamic shadows that dance across the concrete, enhancing the sense of depth and perspective in this tranquil, architectural journey.

c5. The camera smoothly glides around a quaint, enclosed plaza, its cobblestone floor echoing the whispers of history. At the heart of this serene courtyard stands a majestic stone statue, its features meticulously carved, exuding an aura of timeless grace. The surrounding walls, aged and weathered, form a protective embrace, their surfaces adorned with creeping ivy and subtle cracks that tell tales of the past. The light remains constant, casting gentle shadows that dance across the stone, enhancing the statue's dignified presence. As the camera circles, the scene remains tranquil, capturing the essence of stillness and solitude within this hidden sanctuary.

c6. The camera glides smoothly across a sunlit brick courtyard, enclosed by towering, weathered walls, each brick displaying unique textures and subtle color variations. The lens captures the intricate details of the aged brickwork, revealing the craftsmanship of the past. As the camera moves, it focuses on the ornate window frames, their wooden surfaces worn by time, and the sturdy, iron-clad door frames, each telling a silent story of resilience. The fixed exposure and focus highlight the play of light and shadow across the surfaces, creating a serene, timeless atmosphere. The absence of movement in the environment emphasizes the stillness, allowing the viewer to appreciate the architectural details within the ten-meter range.

c7. The camera glides smoothly through a serene, enclosed garden, where towering hedges form lush, green walls, their leaves and branches perfectly still, creating a sense of tranquility. Stone paths weave intricately beneath the camera's gentle orbit, revealing a mosaic of cobblestones and pebbles, each step echoing the garden's timeless elegance. The camera remains low, capturing the rich textures of the hedges, their leaves a vibrant tapestry of greens, while the absence of the horizon enhances the garden's secluded charm. Sunlight filters softly through the foliage, casting delicate patterns on the paths, as the camera continues its graceful, uninterrupted circle.

c8. A steady camera glides through a covered market arcade, capturing the quiet ambiance of closed stalls and rigid awnings. The path is lined with colorful, yet motionless, signs and awnings, each displaying faded logos and names, hinting at the market's bustling past. The camera's smooth movement contrasts with the stillness of the scene, emphasizing the absence of people and activity. The arcade's architecture, with its intricate ironwork and vintage lamps, adds a nostalgic charm. As the camera advances, the muted colors and soft lighting create a serene, almost timeless atmosphere, evoking a sense of calm and reflection.

c9. The camera glides smoothly along a meticulously constructed scaffolding, tightly enveloping a historic masonry facade. The structure's intricate network of vertical poles and horizontal planks creates a geometric maze, inviting the viewer to explore its depths. As the camera weaves through this industrial labyrinth, the surrounding tarps hang still, their surfaces adorned with colorful tags and markings, each telling a silent story of the ongoing restoration. The lighting remains unwavering, casting a soft, even glow that highlights the texture of the weathered stone and the scaffolding's metallic sheen. The only movement is the camera's deliberate journey, capturing the serene stillness of this architectural cocoon.

c10. A deliberate dolly shot captures the side of a parked freight locomotive, its vibrant colors contrasting against the muted tones of a towering retaining wall. The camera glides smoothly alongside the train, revealing intricate details of the locomotive's exterior, from its weathered metal surface to the bold insignia emblazoned on its side. The background remains consistently framed by the high retaining wall and a row of parked cars, emphasizing the train's imposing presence. The scene is serene, with no movement from hoses or cables, allowing the viewer to focus solely on the locomotive's grandeur as

the camera continues its steady slide.

E.3.2. Fast camera movements

c11. The camera embarks on a swift journey through a scaffold tunnel, enclosing a bustling sidewalk, capturing the essence of urban life. The structure, devoid of tarps or fluttering tags, stands rigid and industrial, its metallic framework casting intricate shadows on the ground. As the camera races through, it weaves skillfully between the vertical beams, maintaining a seamless flow within the scaffold's confines. The tunnel's linear perspective creates a mesmerizing visual rhythm, with the steady, unyielding lines of the scaffold contrasting against the dynamic motion of the camera, evoking a sense of speed and precision in this urban passageway.

c12. The camera swiftly navigates through a dimly lit parking structure, weaving through ground-level lanes bordered by imposing concrete walls and sturdy columns. The scene is eerily still, with parked cars, directional signs, and various fixtures frozen in time, creating a stark contrast to the camera's dynamic movement. As it executes two precise, sharp turns, the camera captures the texture of the concrete and the subtle play of shadows, enhancing the sense of speed and agility. The atmosphere is tense yet captivating, with the camera's fluid motion providing a sense of urgency and exploration within the static environment.

c13. In a secluded, ancient stone courtyard, a majestic fountain stands at its center, crafted from weathered marble, its intricate carvings telling tales of old. The camera swiftly arcs around the fountain, capturing every detail of its ornate design, while the surrounding high stone walls, adorned with creeping ivy, create an intimate, enclosed atmosphere. The water within the fountain remains perfectly still, a flawless mirror reflecting the fountain's grandeur and the muted tones of the stone. The rapid camera movement contrasts with the serene, undisturbed water, emphasizing the tranquility and timelessness of this hidden sanctuary.

c14. The camera swiftly navigates through a deserted market arcade, gliding under a series of closed stalls and vibrant awnings, each adorned with colorful, fixed signs. The lighting remains consistently warm, casting a gentle glow over the scene, enhancing the rich textures of the fabric and wood. As the camera accelerates, it executes a graceful S-curve, weaving smoothly between the stalls, capturing the intricate details of the market's architecture. The fixed awnings flutter slightly in the breeze, adding a sense of life to the otherwise still environment, while the constant speed of the camera creates a dynamic, immersive experience.

c15. The camera ascends swiftly up a narrow, dimly lit exterior stairwell, flanked by two towering brick facades, their textures detailed and weathered. The stairwell is a tight, vertical corridor, with each step meticulously crafted from aged stone, worn by time. The walls on either side are adorned with creeping ivy and faded graffiti, adding character to the urban setting. As the camera climbs, the ambient sounds of a bustling city are faintly audible, yet the stairwell remains eerily still, creating a sense of isolation. The ascent is smooth and uninterrupted, with the facades maintaining their imposing presence, emphasizing the confined space and the absence of any distant horizon.

c16. A dynamic aerial view captures a robust freight locomotive, its vibrant colors contrasting against the towering high retaining wall, as the camera swiftly orbits around it. The locomotive, with its intricate details and weathered exterior, stands motionless on the tracks, surrounded by an expansive, quiet rail yard. The camera's rapid circular motion creates a dizzying effect, emphasizing the locomotive's imposing presence and the wall's textured surface. As the orbit tightens, the locomotive's features become more pronounced, showcasing its powerful build and the industrial ambiance of the yard, while the retaining wall remains a constant, looming backdrop.

c17. The camera races through a narrow brick service alley, capturing the gritty details of the urban landscape. The walls, close and confining, are lined with weathered doors, rusted meters, and overflowing dumpsters, each telling a story of the city's hidden life. The bricks, aged and stained, create a textured backdrop as the camera speeds past, maintaining a tight focus to emphasize the claustrophobic nature of the alley. The scene is static, with no movement from the objects, enhancing the sensation of speed and urgency. The alley's dim lighting casts long shadows, adding to the mysterious and slightly ominous atmosphere, as the camera's swift journey continues uninterrupted.

c18. The camera swiftly circles a grand marble statue of a mythological figure, positioned at the heart of a small, serene museum courtyard. The courtyard is enclosed by towering, ivy-covered walls, creating an intimate, secluded atmosphere. As the camera loops rapidly, it brushes past intricately carved stone columns and ornate wrought-iron railings, capturing the play of light and shadow on their surfaces. The statue, bathed in soft, natural light filtering from above, stands as the focal point amidst the stillness, its detailed features and flowing robes frozen in time. The only movement is the camera's dynamic orbit, emphasizing the tranquil, timeless ambiance of the courtyard.

c19. The camera glides swiftly through an expansive underpass colonnade, capturing the rhythmic alignment of towering concrete columns. The scene is devoid of any movement from flags, foliage, or debris, emphasizing the stillness of the environment. The camera's fluid motion creates a seamless journey, weaving gracefully between the columns, maintaining

a steady path beneath the deck. The play of light and shadow on the concrete surfaces adds depth and texture, enhancing the visual experience. The continuous movement offers a mesmerizing perspective, drawing the viewer into the architectural symmetry and the serene, undisturbed atmosphere of the underpass.

c20. The camera swiftly navigates through a labyrinth of towering shipping containers, their vibrant hues of red, blue, and green contrasting against the clear sky. The narrow lanes create a sense of urgency as the camera glides effortlessly, making two sharp ninety-degree turns, each corner revealing a new path. The static containers, adorned with international shipping logos and weathered signs, stand as silent sentinels, their metallic surfaces reflecting the sunlight. The camera's rapid movement through the maze creates a thrilling sense of exploration, capturing the intricate geometry and industrial beauty of the container cityscape.

E.4. Appearance-Complex Prompts

E.4.1. Slow camera movements

d1. A sleek chrome motorcycle stands proudly indoors, its polished surface reflecting the static environment. The camera begins a slow, deliberate orbit around the bike, capturing the intricate details of its curved bodywork. As the camera glides smoothly, stable reflections slide gracefully across the chrome, highlighting the craftsmanship and design. The environment remains rigid and still, with no movement or change in lighting, emphasizing the motorcycle's gleaming surface. The constant exposure and lighting create a serene atmosphere, allowing the viewer to appreciate the motorcycle's elegance and the artistry of its reflective surfaces.

d2. The camera glides smoothly along a wall of glass bricks, each brick capturing and distorting the static room beyond with mesmerizing refractions. The bricks, arranged in a precise grid, create a kaleidoscope effect, bending light and subtly altering the view of the room's muted tones and simple furnishings. As the camera maintains a constant distance, the glass bricks reveal a dance of light and shadow, with each brick acting as a lens, offering a unique perspective of the stillness beyond. The gentle dolly movement emphasizes the serene, unchanging nature of the room, while the glass bricks transform the ordinary into a captivating visual symphony.

d3. The camera glides smoothly across an intricate mosaic floor, capturing the mesmerizing dance of geometric patterns and vibrant colors. Each tile, a unique piece of art, is meticulously arranged, creating a harmonious tapestry of shapes and hues. The grout lines, precise and unwavering, form a delicate lattice that binds the mosaic together. The camera's shallow angle reveals the subtle texture of the tiles, highlighting their glossy surfaces and the occasional imperfections that add character. As the camera slides laterally, the fixed exposure and focus maintain a consistent clarity, allowing the viewer to appreciate the artistry and craftsmanship of the mosaic in exquisite detail.

d4. Inside a serene, dimly lit museum gallery, a camera smoothly advances toward an exquisite display of crystal sculptures encased in pristine glass. The sculptures, intricately carved with precision, stand motionless, their multifaceted surfaces capturing and reflecting the ambient light. As the camera draws closer, the stable specular highlights glide gracefully over the crystal facets, creating a mesmerizing dance of light and shadow. The glass case remains untouched, preserving the delicate artistry within. The steady push-in reveals the intricate details of each sculpture, emphasizing their brilliance and craftsmanship, while the ambient lighting remains constant, enhancing the serene and contemplative atmosphere.

d5. The camera glides slowly along a wire-mesh fence, capturing the intricate lattice of thin metal strands, each intersection forming a precise grid pattern. The focus shifts to the scaffolding joint, where metallic beams intersect, showcasing the industrial elegance of their design. The camera's steady movement highlights the repeating gaps, creating a rhythmic visual pattern. The scene is devoid of motion or distortion, with every element in perfect alignment, emphasizing the rigidity and precision of the structure. The lighting casts subtle shadows, enhancing the texture and depth of the metal surfaces, while the camera's unwavering track maintains a serene, mechanical grace.

d6. The camera glides smoothly over an expansive circuit board, capturing the intricate landscape of technology. It begins at the robust connectors, their metallic surfaces gleaming under soft lighting. As it moves, the lens reveals a network of fine copper traces, like delicate veins, weaving across the board's surface. The journey continues over an array of components: capacitors, resistors, and microchips, each precisely placed, their labels and markings crisp and clear. The board's surface is a sea of green, punctuated by the occasional silver and black of the components. The scene is serene, with no blinking lights or moving parts, emphasizing the stillness and precision of the electronic world.

d7. The camera glides slowly along a perforated metal screen wall, revealing a mesmerizing pattern of repeating circular holes. The oxidized texture of the metal, with its rich hues of rust and patina, creates a tapestry of earthy tones. As the camera maintains a constant angle, the intricate details of the screen's surface become apparent, showcasing the interplay of light and shadow across the perforations. The static surroundings, including a hint of industrial architecture in the background, remain unchanged, emphasizing the serene, rhythmic motion of the camera's lateral journey. The scene evokes a sense of

timelessness and industrial beauty.

d8. The camera begins its slow, deliberate journey toward a meticulously crafted wicker basket resting on a rustic wooden table. The basket's intricate weave, a tapestry of interlocking fibers, becomes increasingly detailed as the camera draws nearer. The ambient lighting casts a warm, golden hue, accentuating the basket's natural tones and textures. The table's rich, grainy surface complements the basket's earthy aesthetic. As the camera continues its steady approach, the basket's craftsmanship is revealed in stunning clarity, each fiber distinct and unmoving, creating a serene, almost meditative visual experience. The focus remains sharp, capturing the essence of artisanal skill.

d9. A sleek, polished black grand piano stands majestically in a spacious, elegantly lit room, its glossy surface reflecting the ambient light. The camera begins a gentle orbit around the piano, capturing the smooth, stable reflections that glide effortlessly across the curved lid, creating a mesmerizing dance of light and shadow. The room is tastefully decorated, with soft, neutral tones that complement the piano's deep black finish. As the camera continues its steady circle, the intricate details of the piano's craftsmanship are revealed, from the delicate curve of its legs to the subtle sheen of its keys. The atmosphere is serene and timeless, with the constant exposure and white balance maintaining a harmonious visual experience, allowing the viewer to fully appreciate the piano's elegance and the tranquil beauty of the setting.

d10. The camera glides slowly across a set of meticulously aligned Venetian blinds, each slat casting sharp, parallel shadows that create a mesmerizing pattern of high-frequency lines. The blinds are illuminated from the left, casting a warm, consistent glow that highlights their rigid structure. The angle remains shallow, emphasizing the precision and uniformity of the slats, which stand perfectly still, devoid of any movement. The steady lighting accentuates the texture and depth of the blinds, while the camera's smooth lateral motion reveals the intricate play of light and shadow, creating a hypnotic visual rhythm.

E.4.2. Fast camera movements

d11. In a sleek, mirrored showroom, the camera embarks on a swift orbit, weaving seamlessly between four towering mirrors. The reflective surfaces, pristine and flawless, capture the dynamic motion, creating an illusion of infinite space. The room's polished marble floor and minimalist decor, featuring a single elegant vase on a pedestal, remain perfectly still, enhancing the sense of motion. As the camera glides rapidly, the mirrors reflect each other, forming a mesmerizing kaleidoscope effect. The ambient lighting casts a soft, even glow, ensuring no flicker disrupts the visual harmony. The rapid movement creates a captivating dance of reflections, maintaining focus within the room's boundaries.

d12. The camera swiftly navigates through narrow aisles of a high-tech server room, where matte black panels line the path, each adorned with steady, glowing indicator lights in hues of green and blue. The atmosphere is silent and still, with the only movement being the camera's agile journey. It executes two precise, sharp turns, maintaining a close proximity to the towering racks, emphasizing the dense, labyrinthine layout. The ambient hum of the servers is palpable, yet nothing blinks or shifts, creating a sense of calm amidst the technological maze, as the camera's fluid motion contrasts with the static environment.

d13. A sleek, high-definition lateral sweep across a set of Venetian blinds, each slat meticulously aligned, captures the essence of motion and light. The blinds, illuminated from the left, cast sharp, rhythmic shadows, creating a mesmerizing pattern of light and dark. As the camera glides smoothly from one end to the other, the steady illumination highlights the precision of each slat, emphasizing the aliasing effect. The blinds remain perfectly still, their metallic sheen reflecting the consistent light source, while the camera's swift, unwavering movement creates a dynamic visual experience, showcasing the interplay of light, shadow, and motion.

d14. The camera embarks on a dynamic journey through a complex network of aluminum pipes, suspended intricately beneath a vast factory ceiling. The pipes, gleaming under industrial lights, form a maze of intersecting pathways at diverse heights, creating a labyrinthine structure. As the camera weaves swiftly through the rigid, motionless framework, it navigates tight corners and narrow passages, offering a thrilling perspective of the metallic landscape. The pipes' polished surfaces reflect the ambient light, casting intricate shadows on the factory floor below, enhancing the sense of depth and complexity in this industrial marvel.

d15. The camera swiftly tilts and dollies around a grand glass display case, filled with an array of dazzling cut gemstones, each facet catching the light with precision. As the camera circles one corner, the gems remain perfectly still, their vibrant colors and intricate cuts highlighted by consistent specular reflections. The brisk movement of the camera creates a dynamic perspective, emphasizing the brilliance and clarity of the gemstones. Exiting to a wider view, the display case stands majestically in the center of an elegant showroom, its contents shimmering under the soft, ambient lighting, inviting admiration and awe.

d16. The camera ascends a meticulously crafted spiral staircase within a lattice tower, composed of slender, interwoven steel members. The structure's geometry is precise, maintaining a consistent radius as it spirals upward, creating a mesmerizing visual rhythm. The steel members are rigid and unwavering, their linear forms intersecting at calculated angles, forming a

harmonious lattice pattern. The lighting is steady, casting soft, even illumination across the metallic surfaces, highlighting their sleek, industrial elegance. As the camera climbs, the viewer experiences a seamless ascent, the tower's intricate design unfolding in a continuous, hypnotic motion, evoking a sense of infinite elevation.

d17. The camera swiftly glides along a gallery wall, capturing a dynamic sequence of framed fine-text posters and signage, each meticulously aligned. The frames, rigid and unyielding, display intricate typography and vivid graphics, their details momentarily blurred by the rapid motion. The shallow grazing angle accentuates the depth and texture of the wall, creating a sense of urgency and fluidity. As the camera races past, the posters remain unchanged, their content a constant amidst the motion. The sequence culminates in a precise halt, centering on a prominent frame, its text and imagery now in sharp focus, inviting contemplation and appreciation.

d18. The camera swiftly navigates through a labyrinth of hanging beaded curtains, each strand composed of shimmering glass spheres that catch and reflect ambient light in a mesmerizing dance of colors. As the camera weaves between two parallel strands, the beads remain perfectly still, their reflections creating a kaleidoscope of stable, prismatic patterns. The journey continues with a fluid motion, the camera gliding effortlessly past the strands, capturing the intricate details of each glass sphere. Finally, the camera exits gracefully past a sleek display plinth, leaving behind the serene, crystalline world of suspended glass, where only the camera's movement disturbs the tranquil beauty.

d19. The camera glides smoothly through an expansive hall, where towering tile columns and elegant archways repeat in perfect symmetry, creating a mesmerizing visual rhythm. The tiles, intricately patterned in shades of blue and white, reflect the ambient light, casting subtle shadows that dance across the floor. As the camera performs an S-curve, it remains nestled beneath the grand vaults, capturing the majestic scale and architectural precision of the space. The rigid columns and arches stand immobile, their timeless beauty accentuated by the fluid motion of the camera, which weaves gracefully through the serene, echoing corridor.

d20. The camera glides smoothly through a serene sculpture gallery, where glossy black ceramic pieces rest elegantly on sleek pedestals. Each sculpture, meticulously crafted, reflects ambient light, creating a mesmerizing play of shadows and highlights. The camera weaves gracefully between the artworks, capturing the intricate details and the polished surfaces that mirror their surroundings. As it approaches the gallery's centerpiece, a strikingly intricate sculpture, the camera executes a tight, fluid turn, offering a dynamic perspective of the central piece. Throughout the journey, the sculptures remain perfectly still, their reflections unwavering, while the camera's motion brings the gallery to life.